DETERMINING THE FIELD CHARACTERISTICS RELATED TO TRACTOR DYNAMICS

by

Carroll Eugene Goering

A Thesis Submitted to the
Graduate Faculty in Partial Fulfillment of
The Requirements for the Degree of
MASTER OF SCIENCE

Major Subject: Agricultural Engineering

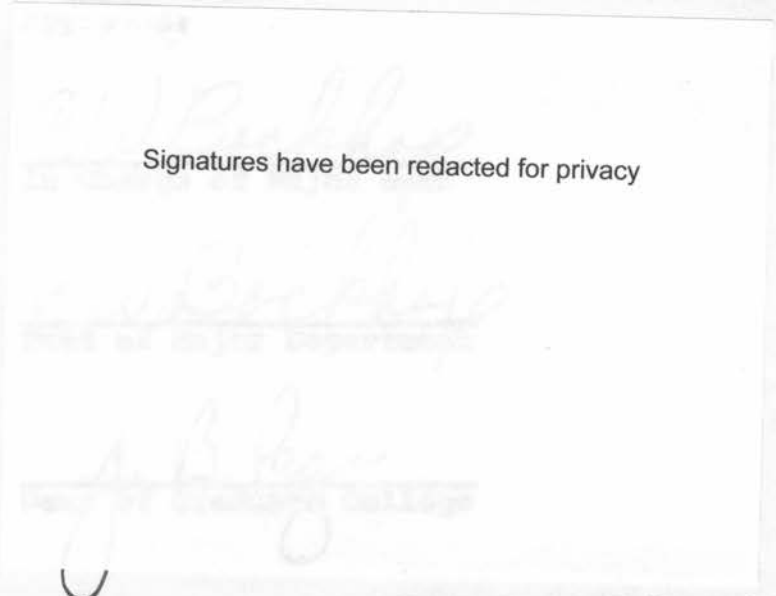

Iowa State University
Of Science and Technology
Ames, Iowa

1962

TABLE OF CONTENTS

LIST OF FIGURES

LIST OF TABLES

INTRODUCTION

In recent years, operator-comfort aspects of farm equipment have become increasingly important. Farmers have demonstrated a willingness to pay extra for such things as deluxe seats, operator cabs and even cab air-conditioning. The response of farm equipment manufacturers to this situation has varied. For example, most manufacturers have made at least some tractor seat improvements. Some have devoted extensive development programs to seat improvement. Morrison and Harrington (11), in reporting on their company's seat development program, raised the point that higher tractor operating speeds may impair operator comfort and human efficiency. Faster travel speeds result in a rougher ride. As new tractors become increasingly powerful, the tendency is to utilize this power with higher operating speeds and thereby avoid traction limitations. Consequently, greater operator discomfort problems may be forthcoming unless operator-station improvements keep pace with tractor power increases.

The alternative to improving the comfort features of the operator station is to take the operator from the tractor and to control the tractor remotely. While remote controlling is technically possible, it appears likely that tractors will be manually controlled for some years to come. Thus an investigation of the comfort aspects of farm equipment is appropriate.

There are many complex factors which determine the state

of comfort of a tractor operator. For example, noise, dust, extreme heat (or cold), and vibration can be identified as factors conducive to discomfort. Considering only one of these, vibration, one can identify engine unbalance and field roughness as sources. Tractor dimensions, weight distribution and tire characteristics further influence the nature of vibration which reaches the tractor operator. The mental and physical characteristics of the operator are also factors.

It would be desirable to study operator comfort in the laboratory, where the numerous factors involved could be individually controlled. Minute tractor design changes could then be accurately evaluated in the laboratory, while the final design could be checked in the field. However, simulation of field conditions must be possible, if operator comfort is to be studied realistically in the laboratory.

One of the most difficult field conditions to simulate is field roughness. Obviously, simulation of field roughness requires a knowledge of how rough fields are; that is, it would be desirable to have quantitative description of the roughness of surfaces over which farm tractors are operated. Unfortunately, no published field roughness data are now available.

Field roughness data should describe the effective, not the undisturbed, field surface. In the field a tractor tire will bridge over some crevices and crush down some clods. The

effective field surface may be defined as that surface which is traced out by the tire bottom as the tractor traverses the field.

This report deals with the development of a technique for collecting effective field roughness data, and with some of the results obtained.

OBJECTIVES

The objectives of this study were:

1. To develope a means for measuring effective field surface roughness.

2. To apply this means to the measurement of roughness patterns in some common agricultural fields.

3. To analyze these patterns and to present the range of conditions encountered.

REVIEW OF LITERATURE

Much literature exists which is pertinent to tractor operator comfort. However, no one has yet systematically investigated one of the principal sources of discomfort--field roughness.

Janeway (8), Zeller (19), Postlethwaite (12), and Jacklin and Liddell (7), have all reported on the reactions of humans to vibration. These reactions were generally determined by subjecting people to sinusoidal vibration of varying amplitude and frequency. The subjects were asked to judge the severity of the vibration. Haack (5) has summarized the results of these investigations. Despite the fact that all results were based on opinion, the results are fairly consistent. For vertical vibration, the frequency range 1 to 60 cps has been divided into three sections. In each section a different motion characteristic governs the intensity of sensation of vibration. Numerical scales for the intensity of sensation have been established.

In all of these tests, it was obviously necessary to limit vibration intensities to safe levels, since human subjects were used. More severe tests have been conducted on animals (15). The work of Coerman et al. (1) holds promise of circumventing present limitations of human reaction tests. They are attempting to describe the human body in terms of a mechanical model. Such a model could be vibrated to destruc-

tion. The resulting data could then be used to predict destructive levels of vibration for humans.

Roesegger and Roesegger (14) have investigated the health effects of tractor driving. They have found that prolonged shock and vibration can have harmful effects on the stomach and the spine of the tractor driver.

Both Loeb (9) and Hornick (6) have found that low frequency vibration can affect visual acuity. Hornick also found that low frequency vibration can impair compensatory tracking (steering) ability.

Dupuis (4) conducted an extensive investigation of vibrations in tractors on test stands. His purpose was to answer basic questions about the effect of vehicle vibrations on the man, and to arrive at conclusions which would aid in the design of better seating facilities. He was also seeking to develop a testing method which would permit exact comparative tests on various seats. Dupuis used wood bumps mounted on a treadmill to simulate roughness. He attempted to relate his simulator roughness to road roughness, but made no attempt to measure field conditions.

Raney et al. (13) established a mathematical model for the vibration of a farm tractor. Certain simplifying assumptions were made, as follows:

1. The tires act as linear springs which have point contact with the supporting surface.

2. The frame and axle of the tractor constitute a rigid body.
3. Small displacements are considered.
4. Three degrees of freedom are assumed:
    a. Vertical displacement of the center of gravity.
    b. Pitch or rotation about the transverse axis through the center of gravity.
    c. Roll or rotation about the longitudinal axis through the center of gravity.
5. Viscous damping only is assumed and this only at each tire.
6. The tractor is assumed to pull or operate no external machinery or implements.

Perhaps the most limiting of these assumptions is the third. Raney used an Oliver Model 550 tractor on a shaker to experimentally check his mathematical model. The sinusoidal input to the tires had to be limited to 0.100 inch peak to peak to prevent the tractor from jumping off the shaker. Obviously, a linear mathematical model is invalid for situations where the tractor tires lose contact with their supporting surface. Thus, the 0.100 inch restriction is a severe limitation. Raney suggests, however, that a non-linear mathematical model might be found which would describe the tractor motion through a wider range of vibrational inputs.

Raney programmed his model on an analog computer. Lacking field roughness data, he used a sine wave generator and a noise generator to furnish inputs to his model. He recommended, however, that an analysis of field conditions be made so that ultimately the tractor vibration could be described adequately for field conditions of operation.

Van Gerpen (17) developed a technique of instrumentation for evaluating tractor seating comfort, and specifically, for measuring jerk (time rate of change of acceleration). He states,

> If a check of riding comfort is to be made using a tractor, then a test track with some form of permanent obstacles should be available. If minute changes in a (seat) suspension are to be made and evaluated accurately, or if reaction to certain types of bumps is to be studied, it is important that these variations be tested under identical conditions.

Van Gerpen did not say how the test track conditions might be related to field conditions.

Various methods exist for simulation of field roughness. Van Gerpen's proposal to use permanent obstacles on a test track represents one method. The treadmill used by Dupuis represents another approach. A third approach is the programming of Raney's mathematical model on the analog computer. In this method, not only the field roughness, but also the tractor itself, is simulated. A fourth approach to the roughness simulation problem is the use of shake tables. Raney used a shake table to experimentally check his mathematical

model. A good discussion of simulation by a shake table can be found in the book, "Random Vibration", by Crandall et al. (2). In this book, the shake table is alternately considered as an energy source, a motion generator, and a failure simulator. The motion generator concept has been found to be the most popular of the three concepts. Shake table design has been influenced accordingly. Although the book, "Random Vibration", considers problems in missile vibration, some of the techniques seem applicable to the problems of simulating agricultural field roughness.

ANALYSIS OF THE PROBLEM

Since most field surfaces are deformable, the shape of an effective field surface depends on the physical characteristics of the vehicle traversing the surface. Thus, measurement of effective field surfaces involves two large categories of factors. These are field factors and vehicle factors. To reduce the number of vehicle factors involved, certain simplifying assumptions were made, as follows:

1. The vehicle is a conventional wheel type farm tractor, equipped with rubber tires.
2. No external machinery is attached to the tractor.
3. Wind, gyroscopic and all other external forces except wheel reactions are negligible.
4. Each tire remains in contact with the field.
5. The forward speed of the tractor is uniform.

Under these assumptions, the only external forces acting on the tractor are those transmitted through the tires. The force transmitted through a given tire depends upon the relative motion between the tire bottom and the tire center. As a tractor crosses a rough field, the vertical displacement of each tire bottom varies with time. When the tractor is considered as a vibrating system, the motions of the tire bottoms constitute the inputs from the field, or the forcing functions. Thus for the tractor shown in Figure 1, the forcing functions are $y_1(t)$, $y_2(t)$, $y_3(t)$, and $y_4(t)$. If all four of

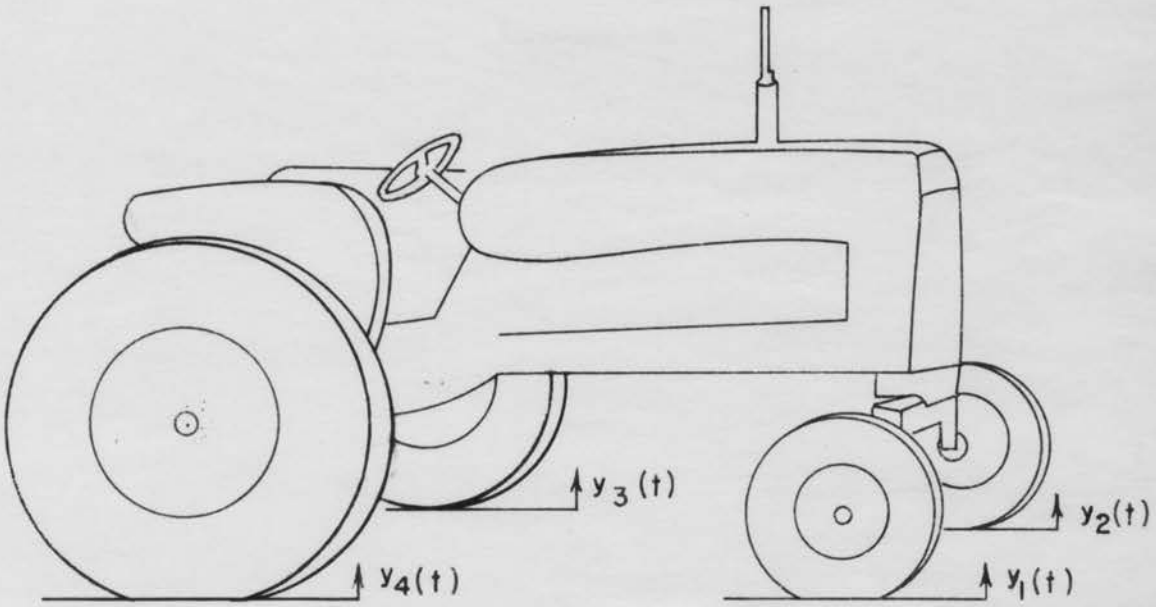

Figure 1. Motion inputs to a tractor crossing rough terrain

these motion inputs from a rough field could be reproduced in the laboratory, the oscillation of the tractor could be reproduced.

In the field, each motion input is generated by the effective field roughness. Thus, to measure the effective roughness "seen" by a given tire, it is only necessary to measure the motion input, y(t), to that tire.

The effective roughness of a given deformable field surface may depend upon several characteristics of the tractor crossing it. The tractor mass, moments of inertia, wheel base, and tire size may all influence the effective roughness of a given deformable field surface. In addition, for a given tractor tire, there are obviously a wide variety of field surfaces which may be encountered. To evaluate the effects of all tractor variables on all types of field surfaces would be quite time consuming.

The approach taken in this project was to limit the number of tractor variables considered in order to increase the number of field conditions that could be investigated in a given time. This approach also helped to reduce the amount of apparatus required in the study. Only one tractor, an Allis-Chalmers D-17 Utility Tractor, was used in the study. This tractor is representative of the average size, general purpose farm tractor. Motion inputs to the right front tire were measured.

INSTRUMENTATION

General Approach

The problem of measuring effective field surface roughness involves the measurement of motion. Either photographic or electrical methods can be used to measure motion. The photographic method would involve the use of a movie camera. A fixed coordinate system would have to be included in the filmstrip as a reference against which motion could be measured. Such reference markers are easily set up in the laboratory, but are inconvenient in the field.

Motion detection and measurement in the field are more easily accomplished by electrical means. The basic instrument employed is a seismic mass type instrument. The inertia of the seismic mass serves as the reference against which motion can be measured. Three types of seismic mass instruments are available. These are vibrometers which measure displacement, velometers which measure velocity, and accelerometers which measure acceleration. Of the three types, only the accelerometer has the inherent lightness and compactness required in this study.

Certain other components must be used to complement the accelerometer. Since displacement is the second integral of acceleration, two integrators must be used to obtain a displacement signal. Amplifiers are required to increase

and maintain the signal magnitude. When low frequency vibrations are being measured, high frequency signal components clutter the acceleration trace. The use of electrical filtering can improve this situation. All of the above-mentioned components are shown in Figure 2, which is a block diagram of the complete instrumentation used to measure field roughness.

The Accelerometer

The accelerometer used in this study was a Statham AJ 17-15-350, temperature controlled, linear accelerometer. The important specifications are:

Axis of Sensitivity	Perpendicular to Base
Ambient Temp. Limits	-65°F to +125°F
Control Temp.	+135°F
Damping at Control Temp.	0.7 ($\pm$ 0.1) of critical
Response to Transverse Accel.	Not more than 0.02 g per g
Acceleration Range	$\pm$ 15g
Non-linearity and Hysteresis	Not more than $\pm$ 1% of full scale excursion
Full Scale Signal Output	$\pm$ 25 millivolts
Natural Frequency	160 cps
Weight	10½ ounces.

The accelerometer was dynamically calibrated. Figure 3 illustrates the results of the calibration for accelerations up to 900 inches/sec^2. The accelerometer has good accuracy within this range. The data on which Figure 3 is based are listed in Table 3, Appendix A.

The rear wheel of a Case tractor was used as the calibrating centrifuge. The important centrifuge features can be

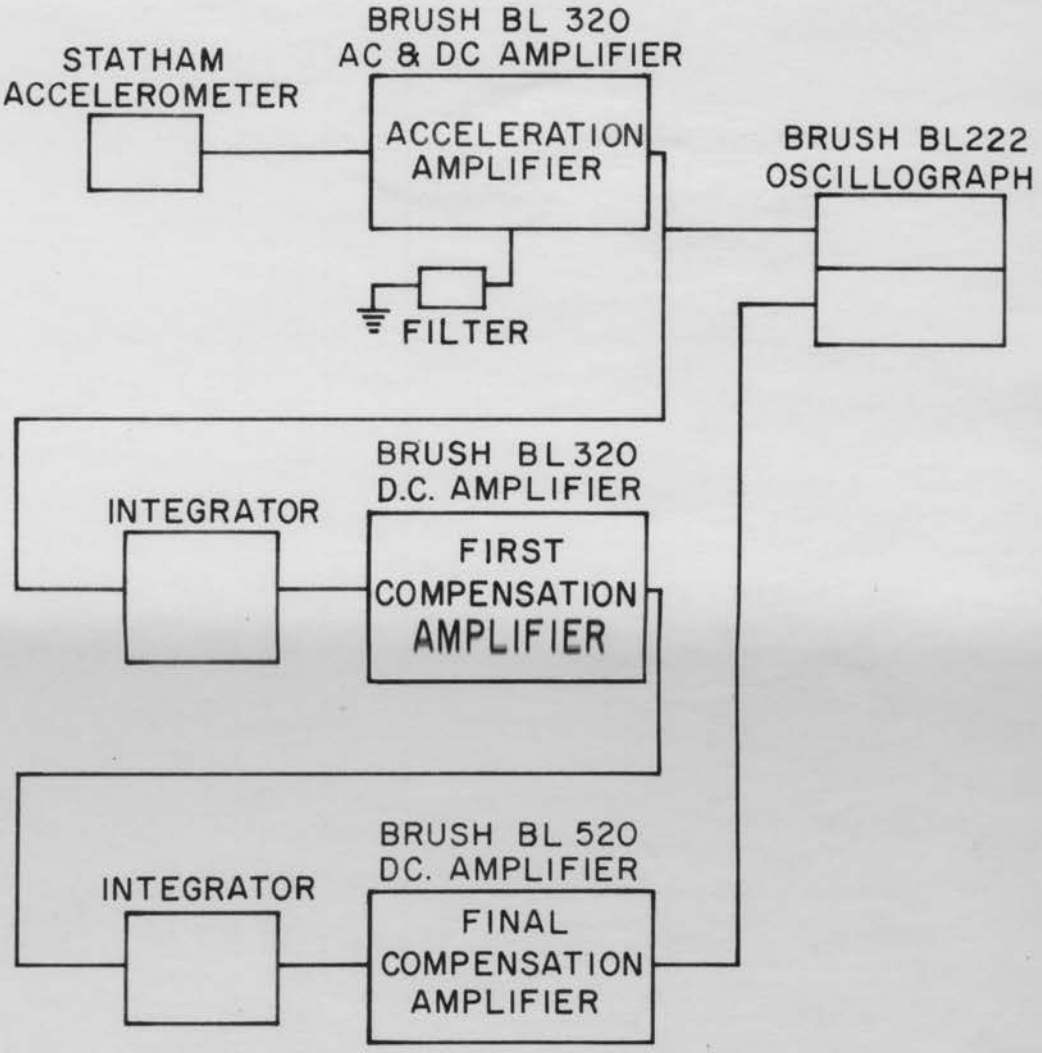

Figure 2. The complete instrumentation used to measure field roughness

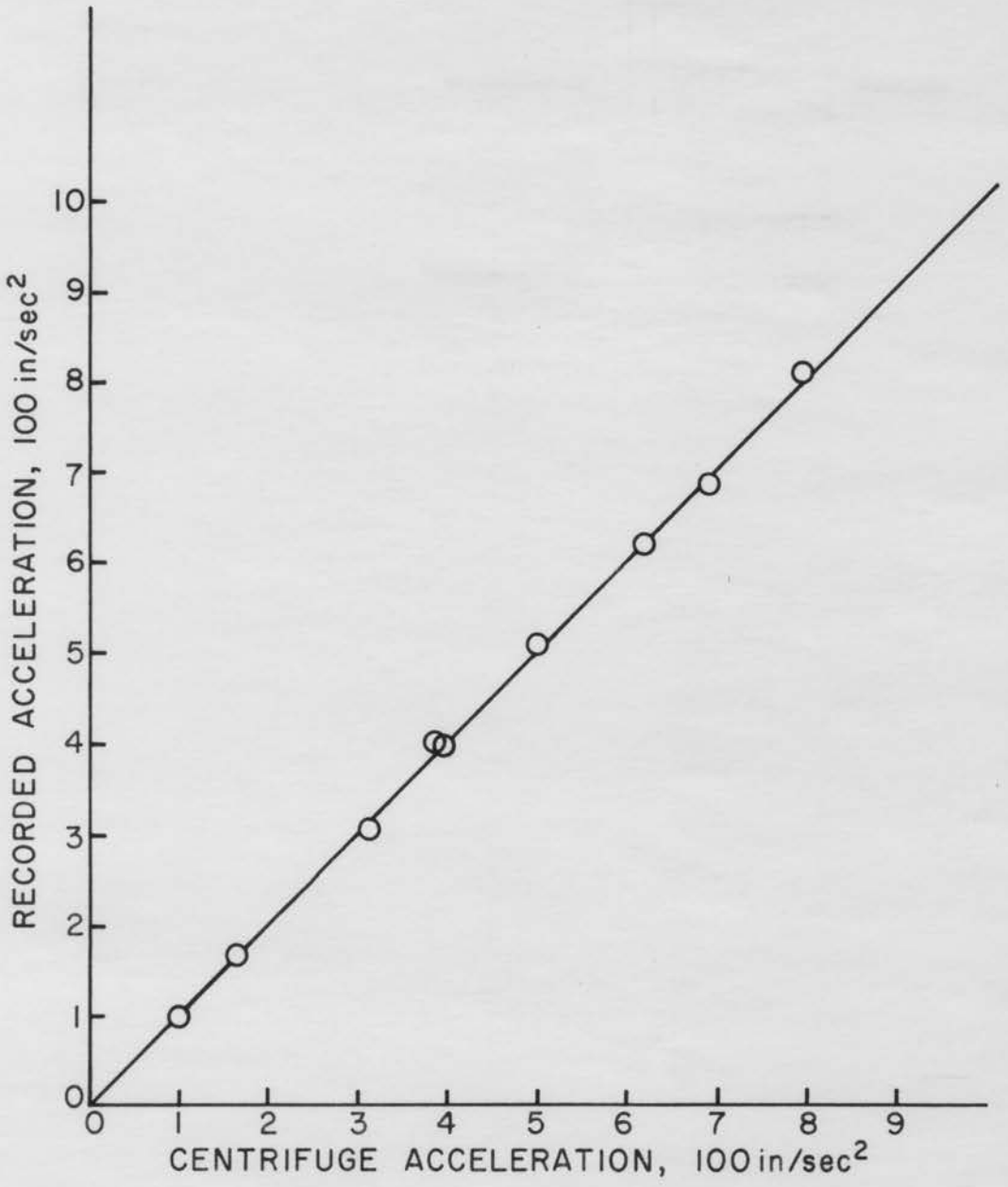

Figure 3. Results of accelerometer final dynamic calibration

seen in Figure 4. A complete description of the entire calibration program can be found in Appendix A.

In Figure 2, the accelerometer is shown connected to a brush amplifier, which in turn is connected to a Brush oscillograph. The maximum sensitivity of the accelerometer-amplifier-oscillograph combination is 10 inches/sec^2 per chart line. This is with the attenuator on the acceleration amplifier set at 1. For any other attenuator setting, the sensitivity in inches/sec^2 per line is 10 times the attenuator reading.

Amplifiers

Three amplifiers were used in this research, as shown in Figure 2. A Brush BL-320 amplifier was used to supply excitation voltage to the accelerometer and to amplify the returning signal. To distinguish it from the other amplifiers, this amplifier will hereafter be referred to as the acceleration amplifier.

The two other amplifiers shown in Figure 2 were used to compensate for signal attenuation by the integrators. The Brush BL-320 in the center was used to compensate for the signal attenuation in the first integrator. Thus, it will hereafter be referred to as the first compensating amplifier. The BL-520 amplifier will hereafter be referred to as the final compensating amplifier.

Figure 4. Dynamic accelerometer calibration using a tractor rear wheel as a centrifuge

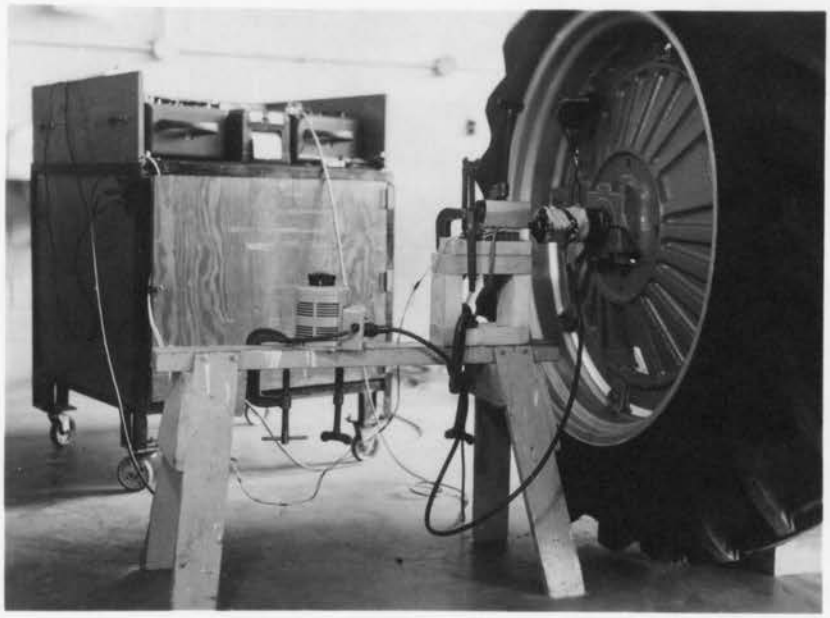

In the acceleration amplifier, both the AC and DC amplifying sections were used. In the compensating amplifiers, only the DC amplifying sections could be used. The AC section of the acceleration amplifier was equipped with a calibrated attenuator. A second calibrated attenuator was available on the DC section of the final compensating amplifier.

The Integrators

The integrating circuits constructed for this study were similar to those described by Thomson (16, p. 99) and by Mitchell (10, p. 198). They are very simple in form, consisting only of a resistor in series with a capacitor. The correct arrangement is indicated in Figure 5. The procedure for selecting suitable resistance and capacitance values is explained in Appendix B.

After the two integrators were constructed, the circuit of Figure 6 was used for final calibration. This circuit is the same as the one shown in Figure 2, except that the accelerometer has been removed and a sine wave generator attached to the DC section of the acceleration amplifier. Since the integrator input was known, the theoretical integrator output could be calculated. As explained in Appendix B, the ratio:

$$\frac{\text{(Wave generator output)}}{\text{(frequency)}^2\ \text{(Integrator output)}}$$

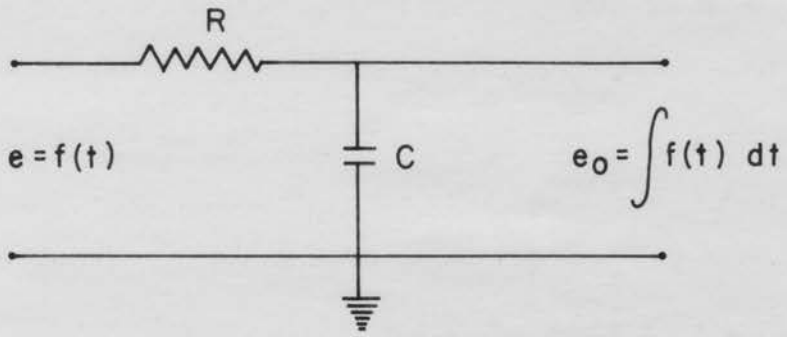

Figure 5. An R-C integrating circuit

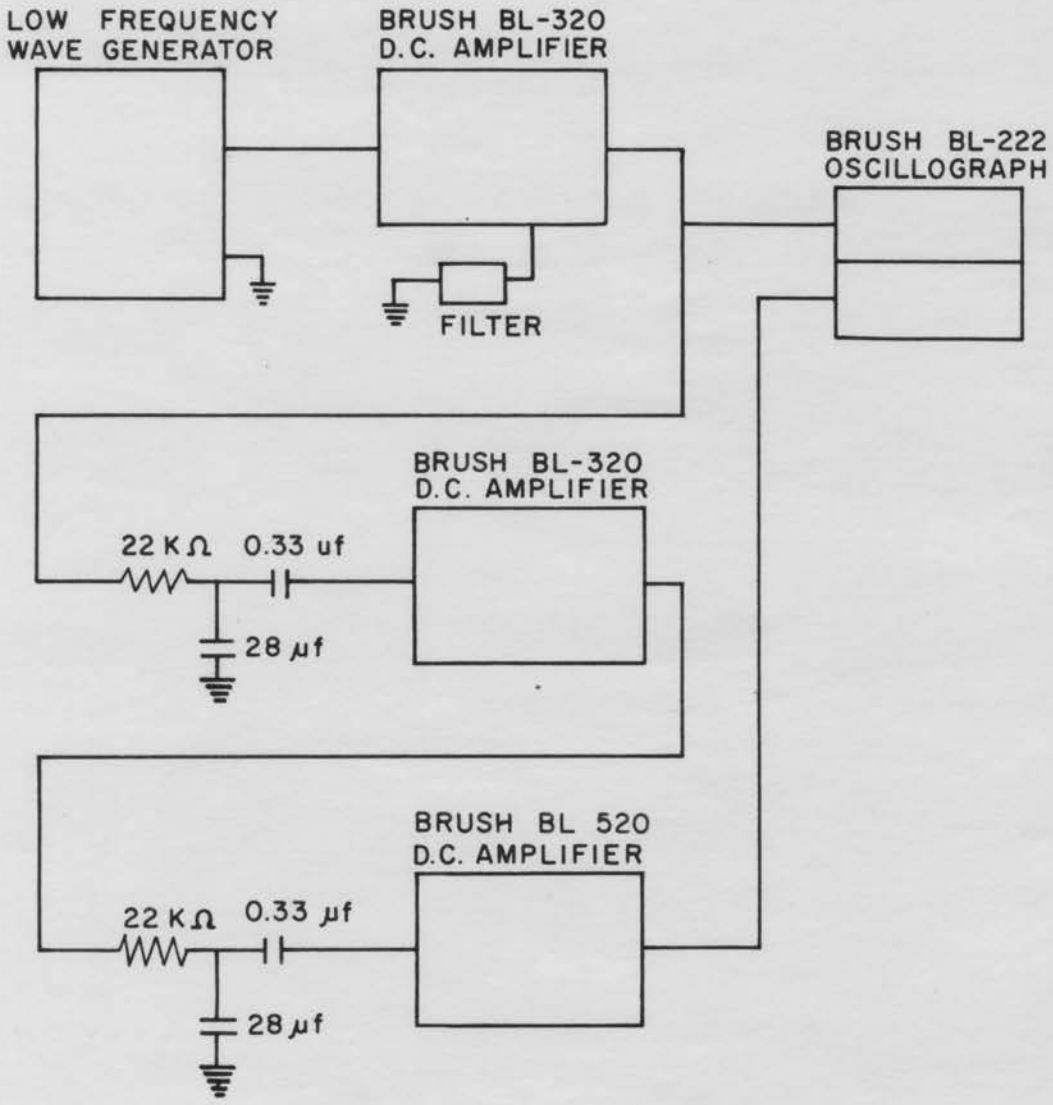

Figure 6. Circuit for final calibration of the double-integrator network

should be a constant for the frequency range over which the integrator is accurate.

The results of the integrator network calibration are tabulated in Table 4, Appendix B. Figure 7 is a graph of these results. Notice that the integrator accuracy decreases sharply below a resistance-to-capacitive reactance ratio of 10. The graph indicates that larger integrating capacitors should have been used for signal frequencies below 2½ cycles per second. The use of larger capacitors would increase the accuracy, and simultaneously increase the signal attenuation. Thus, compensating amplifiers with greater gain would be required. For best results, the compensating amplifiers should each have had a gain greater than 10. The amplifiers available for this study had a gain of approximately 5 so a compromise between accuracy and signal attenuation had to be made.

The displacement sensitivity depends upon the integrator constant of Figure 7, the attenuator setting on the acceleration amplifier, and the attenuator setting on the final compensating amplifier. The derivation of the equation for displacement sensitivity is given in Appendix B. The sensitivity is given by:

$$S_d = (0.00453)\left(\frac{K_d}{0.05}\right)S_a = (0.0453)\left(\frac{K_d}{0.05}\right)K_a$$

where:

S_d = Displacement sensitivity, in/line

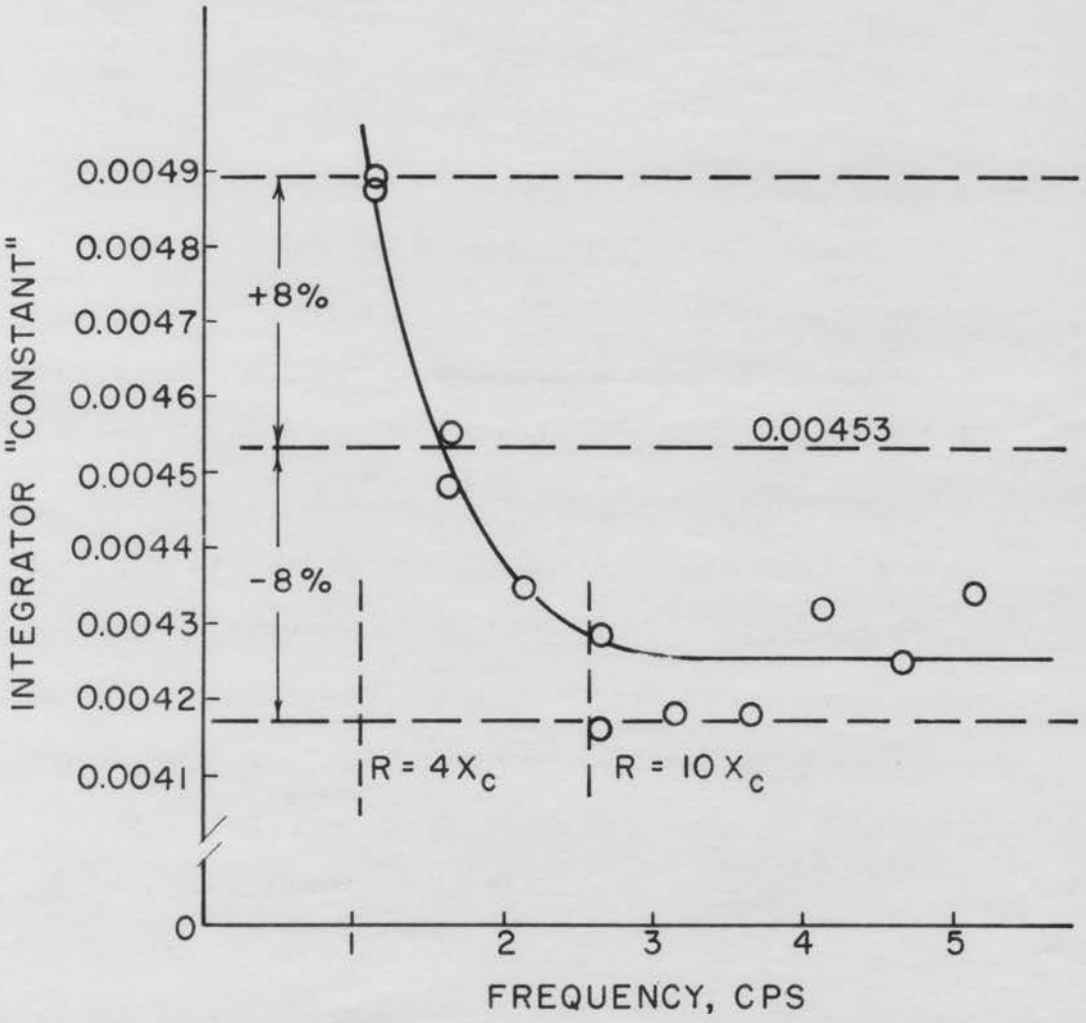

Figure 7. Results of final calibration of double-integrator network

S_a = Acceleration sensitivity, in/sec^2/line.

K_d = Attenuator setting on final compensation amplifier.

K_a = Attenuator setting on acceleration amplifier.

0.00453 = Integration "constant" from Figure 7.

Oscillograph

A brush BL-222 two-channel oscillograph was used for recording purposes. Acceleration was recorded on the one channel and displacement was recorded on the adjacent channel. The oscillograph was equipped with an event marker on one of the channels. The event marker was used to relate oscillograph chart distance to horizontal ground distance.

Filters

The amplitude of acceleration of a sinusoidal vibration increases with the square of the frequency. Thus high frequency noise or engine vibrations have the capability of masking out low frequency vibrations. For example, a 30 cps (1800 rpm) vibration of only 0.01 inch displacement amplitude has the same maximum acceleration value as a 1.0 cps vibration of 9.0 inch displacement amplitude. If low frequency vibrations are to be recorded with an accelerometer, a means of eliminating high frequency components from the signal must be found. For this project, a filtering technique similar to

Van Gerpen's (17) was employed. The acceleration amplifier was modified to obtain sharp attenuation for frequencies over 10 cps, but very little attenuation for frequencies under 10 cps. This was accomplished by adding filtering capacitors to the DC amplifier section, as shown in Figure 8. The dotted lines indicate the connections added to the original circuit. Van Gerpen's lead was again followed in mounting the filtering capacitors outside of the amplifier. This increased flexibility in that the filter could be easily removed, or replaced with a different filter if desired.

The values of capacitance needed were estimated from Van Gerpen's results. Thereafter the capacitance values were varied by trial and error until the desired filtering action was obtained. For this purpose, a function generator was used to deliver a sine wave of constant amplitude and known frequency. The capacitance values listed in Figure 8 were finally selected. Figure 9 illustrates how the filter attenuated a constant amplitude signal as the frequency was increased from 10 to 18 cps.

Event Marker

As previously mentioned, the oscillograph event marker was used to relate chart distance with horizontal ground distance. This was accomplished by connecting a microswitch in series with the event marker and a 6-volt battery. A bolt

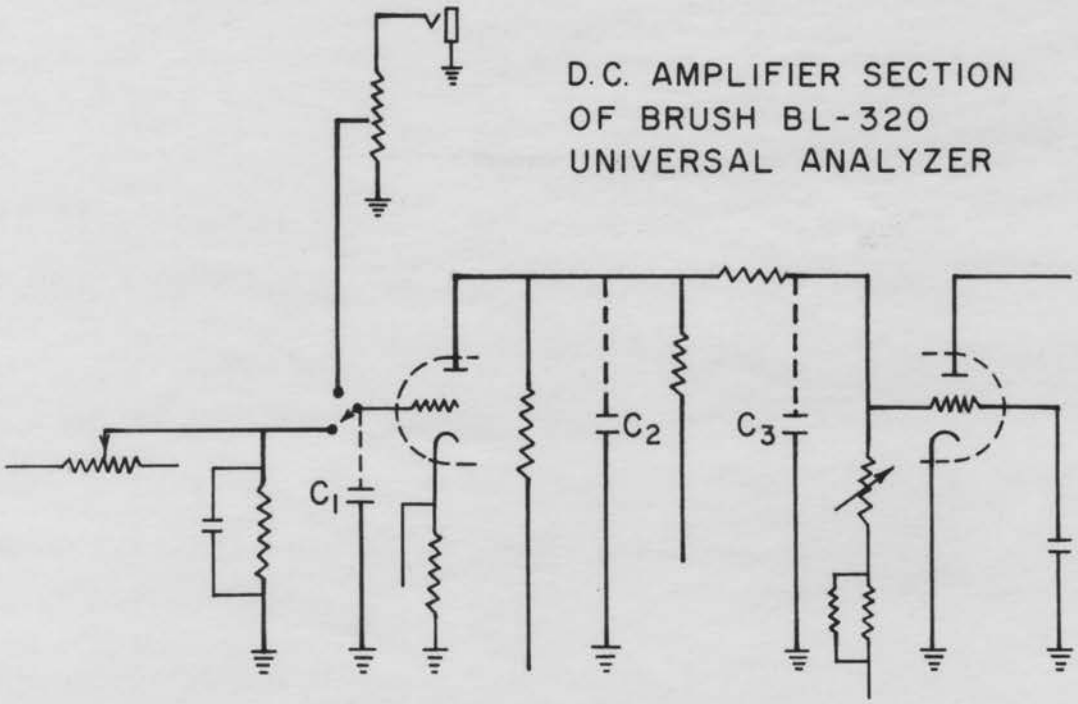

Figure 8. Amplifier circuit changes for attenuation of high frequency acceleration signals

Figure 9. Result of filtering a constant amplitude, increasing frequency sine wave

Figure 10. Microswitch in event marker circuit used for relating oscillograph chart distance to horizontal ground distance

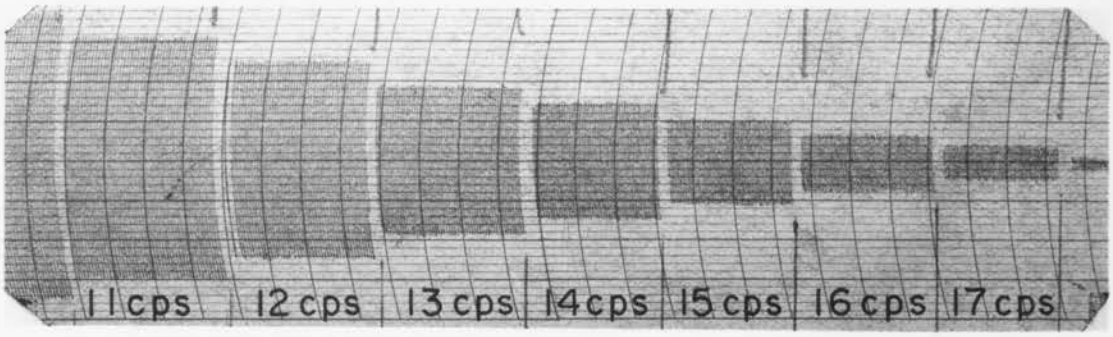
11 cps
12 cps
13 cps
14 cps
15 cps
16 cps
17 cps

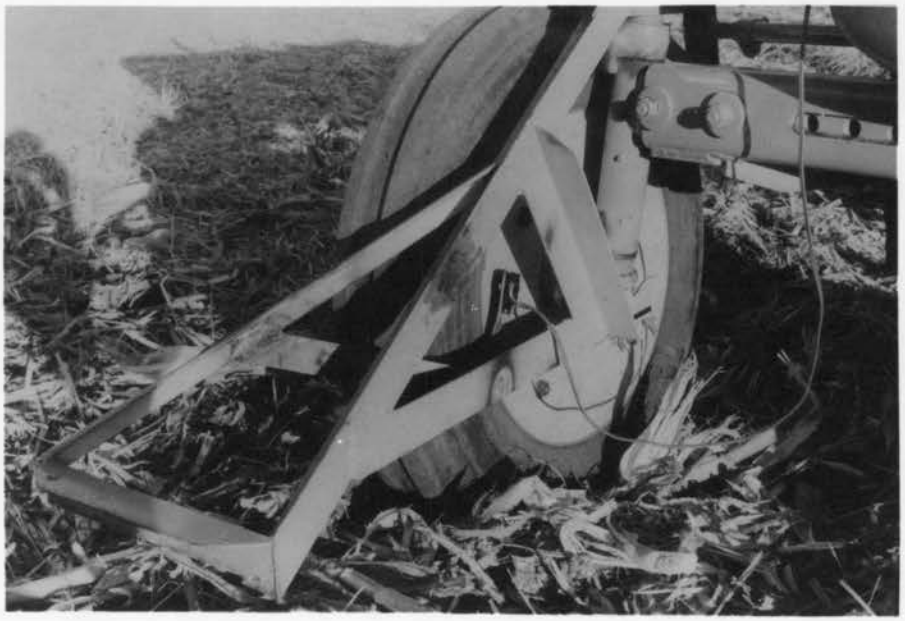

was attached to the front wheel of the Allis-Chalmers tractor used in the field tests. This bolt tripped the microswitch once per wheel revolution. Therefore, knowledge of the effective wheel circumference and of the oscillograph chart speed permitted a correlation of chart distance with ground distance. The location of the microswitch is shown in Figure 10.

Associated Equipment

Several other minor items were required to complete the instrumentation. A portable AC generator was used to supply power in the field. The voltage output of this generator was excessive, so a Superior Type 10B transformer was used to reduce the voltage to 115 V. AC.

The accelerometer temperature was maintained at 135°F by a resistance heater. This heater required a 28-volt AC or DC power source. Consequently, an Ohmite Model VT 2 N transformer was used to reduce the generator voltage to 28 V. AC.

In the field, it was deemed inadvisable to carry all of the instruments over the rough field surfaces. Therefore, most of the instruments were kept in a stationary instrument trailer. The Allis-Chalmers test tractor was operated on a 160-foot diameter circular path around the instrument trailer. To interconnect instruments on the test tractor with equipment on the instrument trailer, several 100-foot cables were

required. A 4-conductor shielded cable was used to interconnect the accelerometer and acceleration amplifier. A three-conductor cable was used to furnish power to the accelerometer heater. A common 2-conductor cable was used to connect the microswitch to the event marker circuit. All cables were attached to a light chain, which was used to carry the weight of the cable assembly between the test tractor and instrument trailer. The cable assembly can be seen in Figure 11.

The Complete System

The instruments carried on the instrument trailer are shown in Figure 12. Figure 2 is a diagram of the key elements in the complete instrumentation system. The system shown had the capability of measuring and recording accelerations and displacements in the frequency range 1 to 10 cps. At frequencies below 1 cps, displacement accuracy was unacceptable (see Figure 7). Signals of frequency greater than 10 cps were attenuated by the filtering system.

In this system, the inertia of the accelerometer seismic mass furnished the reference against which motion was measured. Consequently the displacement recorded on the charts was not referenced to any "bench mark" in the field. Rather, the displacement trace fluctuated around some equilibrium line. This was a satisfactory arrangement, since it was the surface

Figure 11. Test tractor in position to follow a circular path around the instrument trailer

Figure 12. Electronic instruments carried in the instrument trailer

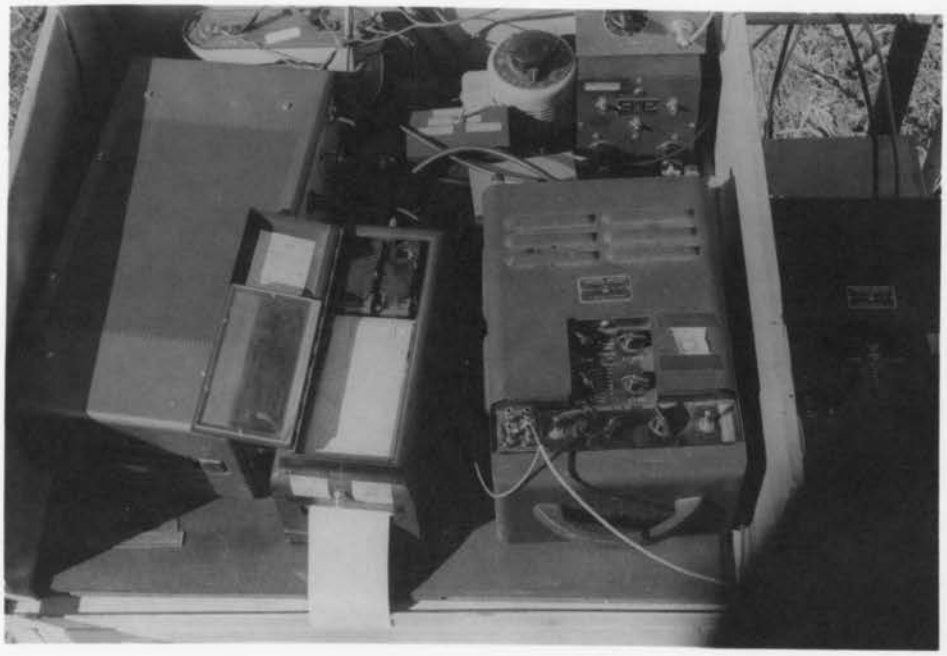

variation which was of interest and not the absolute height of each point relative to some "bench mark."

APPARATUS

Tire Feeler Device

To measure the motion input to a tractor tire, some means is required for connecting the accelerometer to the tire bottom. Direct attachment is impractical. The accelerometer has to remain upright, and in contact with the portion of the tire directly below the wheel center. Thus, the accelerometer must be attached to some intermediate device, which in turn rides against the tire bottom.

The test tractor was equipped on the front end with Firestone Guide-Grip Tractor tires. The ridged profile of these tires offered the possibility of using feelers to follow the motion of the tire bottom. Consequently, the device shown in Figures 13 and 14 was constructed. The universal joint at the front and the spring in the rear serve to maintain contact between the feelers and the tire. Each feeler also prevents the other from moving laterally with respect to the tire. The universal joint and the spring are anchored to a frame which pivots with the wheel. This frame can be seen in Figures 10 and 14. The universal joint allows the feelers to maintain contact when the tire deflects.

The feelers consist of 3/8ths-inch diameter steel rods. To reduce drag on the wheel, the rods were polished. Also, only enough spring tension was used to maintain feeler

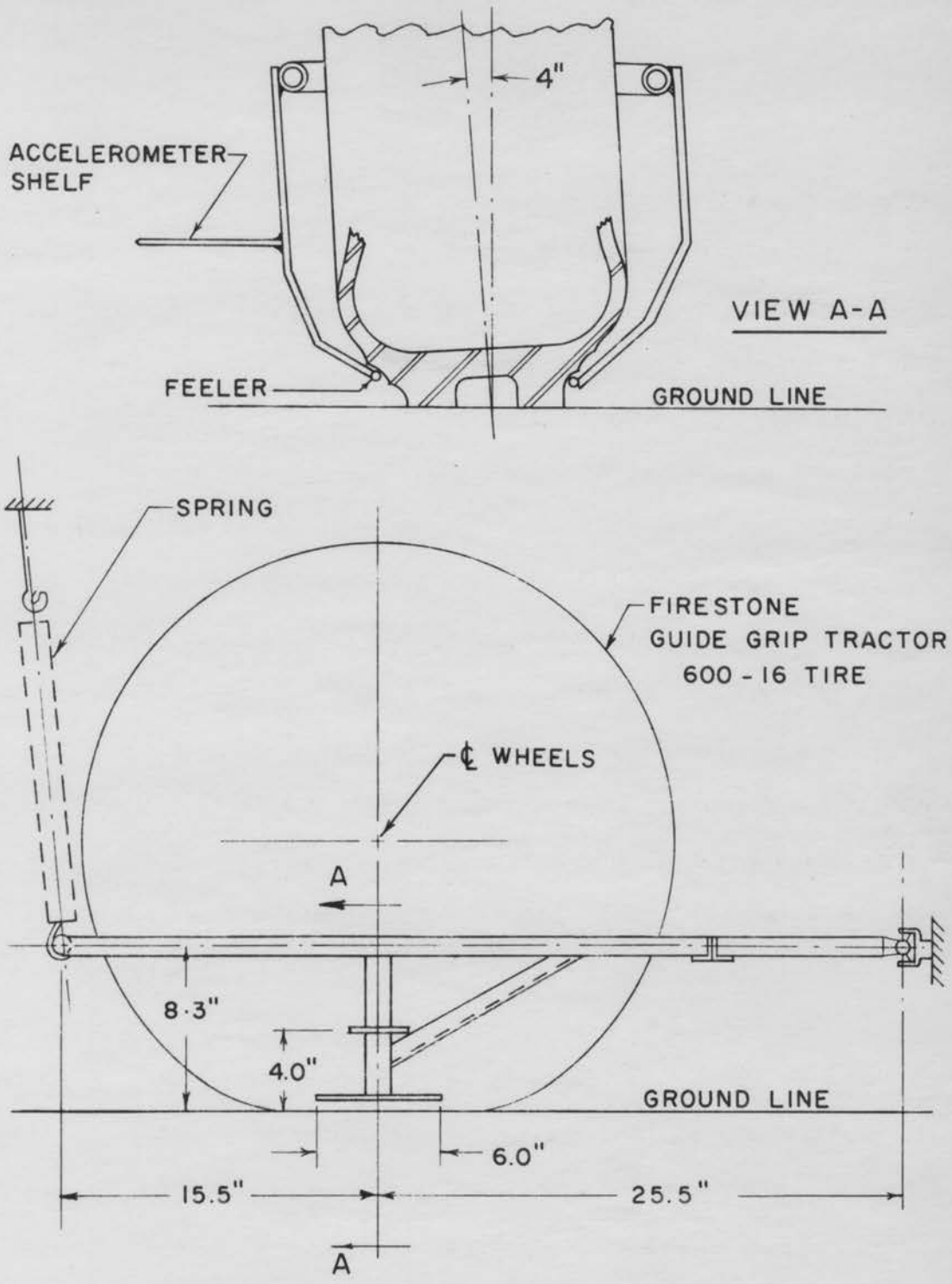

Figure 13. Tire feeler device

Figure 14. The tire feeler device in the field

contact with the tire.

The feeler length was chosen arbitrarily. A six-inch feeler spanned most of the tire contact area. At the same time, each feeler was short enough to maintain total contact with the tire at small tire deflections.

Reference to Figure 13 will aid in an understanding of the utility of the feeler device. The normal to the accelerometer shelf is always perpendicular to the feelers and to a line through the two front wheel centers. With the tractor at rest on a level surface, the normal also intersects the line through the wheel centers. As the tire flexes, the normal oscillates fore and aft across the line through the wheel centers. For the usual tire flexing occurring in the field, these oscillations are small. The shelf normal and the accelerometer axis of sensitivity are parallel. Thus the accelerometer detects motion of the tire bottom approximately along the bottom dead center radius of the tire. This motion constitutes the vibrational input to the tire in the field.

The feeler assembly could be completely removed in the field without the aid of a jack. This could be accomplished by removing seven bolts.

In early field trials, some difficulty was encountered in keeping the tire feelers in the proper grooves on the tire. Particularly in soft, plowed fields, soil pushing against the

supporting structure would tend to force the feelers up onto the sides of the tire. Consequently, another means was sought to measure effective roughness of these soft fields.

Bicycle Wheel Device

The device of Figure 15 represents another approach to the problem of measuring effective field roughness. This approach is based on the assumption that a given deformable bump would impart essentially the same motion to two wheels of similar diameter if their unit contact pressures were equal.

As the bicycle wheel in Figure 15 moves up and down relative to the tractor, the spring stretches and contracts. However, the geometry of the device was selected to give essentially constant tire contact pressure through a tire vertical-displacement range of $\pm$ 4 inches.

Each tire was assumed to have an elliptically shaped contact surface. Thus the contact areas could be calculated from the lengths of the major and minor axes of the contact surface. This assumption of elliptical contact surfaces has previously been used by Vandenberg et al. (18). The lengths of the major and minor axes were determined by a sanding technique. With the tire at rest, fine sand was thrown around the tire periphery. The tire was then removed from the surface, and the major and minor axes were measured.

A large platform scale was used to determine each wheel

Figure 15. Bicycle wheel device for measuring effective field roughness

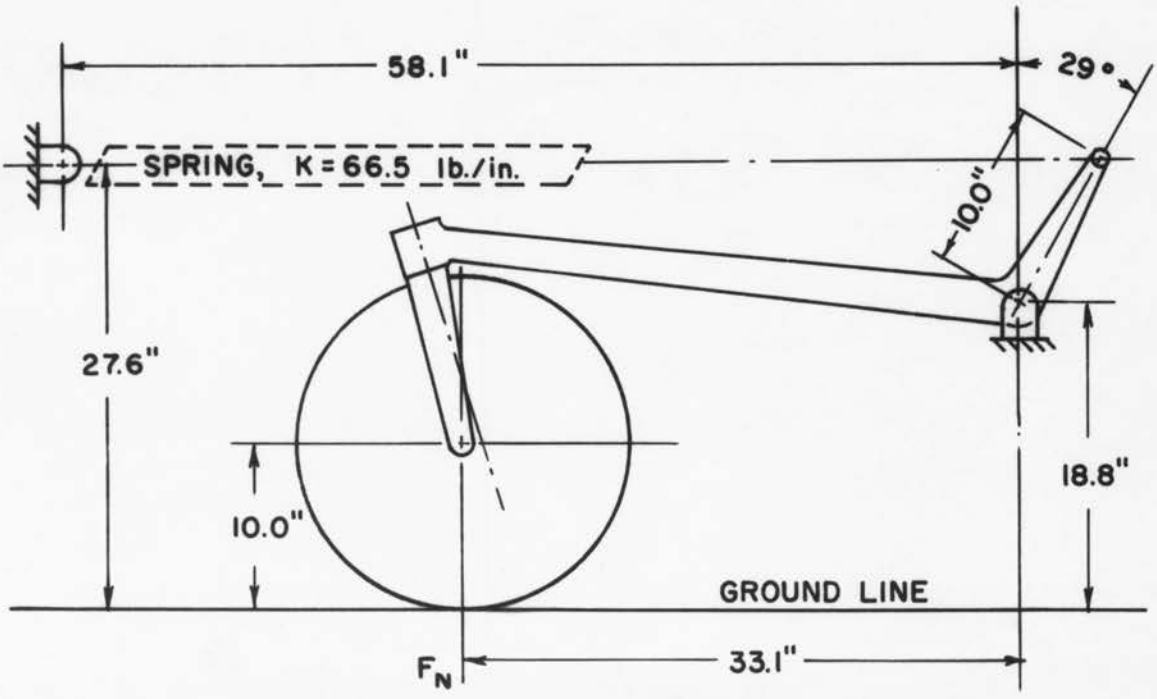
58.1"
29°
SPRING, K = 66.5 lb./in.
10.0"
27.6"
10.0"
18.8"
GROUND LINE
F_N
33.1"

reaction of the Allis-Chalmers tractor. Each front wheel static reaction was found to be 885 pounds. By trial-and-error procedure, a value of 160 pounds was selected for the bicycle wheel reaction. Tire pressures of 30 psig were maintained both in the tractor front wheel and in the bicycle wheel. Under the above conditions, the actual contact pressures varied with the supporting surface. On concrete, the average contact pressure for the tractor tire was 38 psi, for the bicycle tire, 33 psi. On a plowed field, the values were 16 psi and 15 psi, respectively.

The outside diameter of the bicycle wheel was 20 inches. The outside diameter of the front tractor tire was 28 inches.

The accelerometer was mounted at the axle of the bicycle wheel, as shown in Figure 15. It is evident that the accelerometer motion differs from the tire bottom motion by an amount attributable to the tire deflection. However, the bicycle tire was water filled. The small size of the tire coupled with the water-fill nearly eliminated tire deflection.

The natural frequency of vibration of this device is important. The natural frequency must be high enough to minimize excitation by field roughness. It was found that the bicycle wheel would oscillate vertically in free vibration with a frequency of 23 cps. This was satisfactory, since electrical filtering was used to attenuate signals with frequency greater than 10 cps.

The bicycle wheel was designed to caster on corners or curves. This castering gave trouble in the field. In rough fields, the bicycle wheel would often caster 90° to the direction of travel. To prevent excessive castering, stops were placed to limit the castering to a fairly narrow sector.

The lateral location of the bicycle wheel on the tractor can be seen in Figure 16. The bicycle wheel did not follow the track of the front wheel. Rather, it followed a fresh path over the undisturbed field surface.

Figure 16. Lateral location of bicycle wheel in relation to tractor front wheels

DATA COLLECTION

The first step in data collection was the selection of test fields. All of the data were taken on the Iowa State University farms just south of Ames. All of the data were taken in October, 1961, during the harvest season. Consequently, data taking in a particular field was always withheld until the crop was removed. Beyond this, fields were selected to give a variety of roughness conditions. Thus data were taken in two corn fields, two plowed fields, a ridged red-clover field, a soybean field and a meadow. For purposes of identification, the fields were numbered 1 through 7. A description of each field can be found in Appendix C.

Soil moisture samples were taken in fields 2 through 7, but not for the purpose of relating roughness to soil moisture. The moisture samples were taken only to obtain a general measure of the field conditions.

The tire feeler device (Figure 14) was used to measure roughness in all fields except 2 and 3.

The throttle on the Allis-Chalmers tractor was marked, so that the same tractor speed could be used on successive days of data taking. The throttle setting was for approximately three miles per hour forward speed. At this speed, the tractor was able to traverse all of the test fields without the tires losing ground contact.

On the last day of data taking, several extra runs were

made at a higher tractor speed. The speed for these extra runs was approximately six and a half miles per hour.

For each run using the tire feeler device, an accompanying run was made in which vertical motion was measured at a point on the tractor front axle directly over the wheel center. These latter runs were made to obtain some indication of how motion at the axle compared to motion at the tire bottom.

Data were taken on six different days. A standard procedure was followed on each day of data taking. For the initial run, the instrument trailer was parked in the center of the test area. Test areas were selected which were on fairly flat slopes. Then the generator was started, and the amplifiers were allowed to warm up for at least twenty minutes. During this period, the tractor was moved to the periphery of the path to be followed. The cables between instruments on the trailer and instruments on the tractor were connected, and the microswitch for the event marker system was installed on the tractor wheel. The accelerometer was leveled for initial balancing. After the amplifiers were stabilized, the accelerometer bridge was balanced with the balancing controls on the acceleration amplifiers. The accelerometer was then mounted on the tire feeler, bicycle wheel or tractor axle. Motion was then recorded as the tractor was driven halfway around the circle. A half circle constituted a run.

At the end of the run, a run number was written on the

chart record. This number was also entered on a data sheet. The accelerometer location, instrument settings, tractor speed and field description were also entered on the data sheet. A field data sheet is shown in Appendix D.

Subsequent runs followed a similar pattern. Of course, no amplifier warm-up was required on subsequent runs. Also, the accelerometer bridge was balanced only before the initial run. After the tractor had completed one circle, the circle radius was shortened slightly to permit a second circle with a new track.

A system was devised for determining tractor direction of travel from the charts. The event marker was tripped several times in quick succession as the tractor moved perpendicular to the plowing or row direction. After a run, these points on the chart were identified with a note. Consequently, it was later possible to estimate the tractor travel direction at any point on the chart.

DATA ANALYSIS

Surface Classification

The field surfaces encountered fall into two general categories. The first category includes all row crop field surfaces. For these fields, row profiles are easily identifiable on the oscillograph data charts. Furthermore, the row profiles appear to be fairly uniform in size and spacing.

The second category of surfaces includes all non-row crop field surfaces. For these surfaces, no set pattern can be distinguished. Instead, the bumps appear to be randomly arranged.

Row Crop Fields

If the size, shape and spacing of all row profiles in a field were identical, the surface could be described as periodic. A corn field does not have an exactly periodic surface, because some differences do exist between individual row profiles. The surfaces of row crop fields could appropriately be labeled quasi-harmonic.

The row peaks seemed to be the most likely segments of the row profiles to have some definite location. Consequently, the effective surface profile between two adjacent row peaks was considered to be one wave.

For each run, several comparisons were made on six

sequential waves. The six waves chosen were those centered about the point where the tractor was moving perpendicular to the row direction. Because of the large radius of the tractor path, the tractor was traveling essentially perpendicular to the row direction for all six waves.

The first comparison made on each set of sequential waves was a comparison of wave lengths. For each wave, the horizontal distance from crest to crest was measured on the oscillograph chart. Next the average spacing between event marks on the chart was determined. The effective wheel circumference was determined as explained in Appendix E. Using these factors, each wave length was then calculated by the following formula:

$$L = \frac{\rho\lambda}{\delta}$$

where L was the wave length in inches, ρ was the effective wheel circumference in inches per revolution, λ was the crest horizontal spacing in millimeters, and δ was the distance between event marks in millimeters per revolution. For each set of six waves, the mean wave length, standard deviation and coefficient of variation were also computed. In addition, the average tractor speed during the run was calculated by the formula:

$$V = \frac{\rho\gamma}{17.66}$$

where V was the tractor speed in miles per hour, and γ was the

oscillograph chart speed in millimeters per second.

The second comparison on each set of waves was a comparison of amplitudes. For each wave, the average crest height above an arbitrary reference was determined. From this average was subtracted the trough height above the same reference line. The difference was equal to the double amplitude of the wave in millimeters. Multiplication by the displacement sensitivity then gave the wave double amplitude in inches. The mean double amplitude, standard deviation and coefficient of variation for the six waves were then calculated.

To compare wave shapes, a harmonic analysis was made on each wave. The results of these harmonic analyses established a numerical basis for comparing shapes of the waves. The harmonic analysis used in each case was the well-known Fourier analysis. A complete description of the technique may be found in Den Hartog's (3) "Mechanical Vibrations". A summary of the technique follows here.

An arbitrary wave of length L can be described by a trigonometric series of the form:

$$y = f(x) = a_1 \sin\left(\frac{2\pi x}{L}\right) + a_2 \sin 2\left(\frac{2\pi x}{L}\right) + \cdots + a_n \sin n\left(\frac{2\pi x}{L}\right) + \cdots + \frac{b_0}{2} + b_1 \cos\left(\frac{2\pi x}{L}\right) + b_2 \cos 2\left(\frac{2\pi x}{L}\right) + \cdots + b_n \cos n\left(\frac{2\pi x}{L}\right) + \cdots . \quad (1)$$

The b_0 term is a constant. The first sine term and the first

cosine term make up the first, or fundamental harmonic. The second sine term and second cosine term make up the second harmonic, etc.; and in general the n^{th} sine and cosine terms make up the n^{th} harmonic. Vertical distance is measured in the Y-direction and horizontal distance in the X-direction. Equation 1 can represent one wave of length L plus an arbitrary number of following waves if the wave form is periodic.

If an analytical expression for $y = f(x)$ is available, the following formulas can be used to determine the coefficients of the sine and cosine terms in Equation 1:

$$a_n = \frac{2}{L} \int_0^L f(x) \sin n\left(\frac{2\pi x}{L}\right) dx \qquad (2)$$

$$b_n = \frac{2}{L} \int_0^L f(x) \cos n\left(\frac{2\pi x}{L}\right) dx. \qquad (3)$$

If, as in this project, no analytical expression is available, the coefficients a_n and b_n must be determined from the experimental waveform. For this purpose, the formulas 2 and 3 can be replaced by the approximate formulas:

$$a_n = \frac{2}{N} \sum_{K=0}^{K=N-1} y_K \sin n\left(\frac{2\pi K}{N}\right) \qquad (4)$$

$$b_n = \frac{2}{N} \sum_{K=0}^{K=N-1} y_K \cos n\left(\frac{2\pi K}{N}\right). \qquad (5)$$

To use formulas 4 and 5, the base line, L, of the experimental

wave is divided into N equal parts. The ordinates at the division points are designated y_0, y_1, y_2, etc. Then the operations indicated by 4 and 5 are carried out.

A definite procedure was established for making the harmonic analyses. First, a horizontal reference line was selected below the lowest trough in the set of six waves. Thus, all points on the wave could be considered positive ordinates, since they were above the zero reference line. For each wave, ordinates were measured at half-millimeter intervals along the chart. These ordinates were then put on data tapes, and a digital computer was used to evaluate the expressions 5 and 6. The digital computer calculated the coefficients a_n and b_n of the first eight harmonics for each wave and printed out these results. The computer also computed the relative importance of each harmonic in contributing to the total amplitude of the wave. For each wave, the initial and final ordinates were averaged to obtain the average peak height above the reference line. From this average, the minimum ordinate (height of trough above reference line) was subtracted to obtain the double amplitude of the wave. Finally, the double amplitude was divided by two to obtain the amplitude of the wave. This amplitude was divided into the amplitude of each harmonic to determine the relative importance of each harmonic in contributing to the total amplitude of the wave.

A constant term was also obtained from the harmonic analysis on each wave. Since the constant term merely indicates the average height of the wave above some arbitrary reference line, an individual constant term has little meaning. However, if several sequential waves are referred to the same reference line, and if the wave form is periodic, the constant terms should be identical for all of the waves. Differences among the constant terms then indicate a lack of periodicity of the waveform.

After the harmonic analyses, waves within a set could be compared on the basis of wave length, amplitude of the total wave, relative contribution of each harmonic to the total wave amplitude, and constant term differences. The results of these comparisons are tabulated in Tables 5 through 16 in Appendix F.

Non-Row Crop Fields

Figure 17 is a sample of oscillograph chart obtained in a plowed field. The +y direction refers to the upward direction, and +x indicates direction of travel. It appears that the bumps are randomly arranged. Furthermore, the bumps show little similarity of size or shape. Of course, it is possible that the trace represents the superposition of a number of fairly uniform waveforms of different frequencies. To check this possibility, it would be necessary to break the wave down

Figure 17. Sample trace obtained in Run 4B1

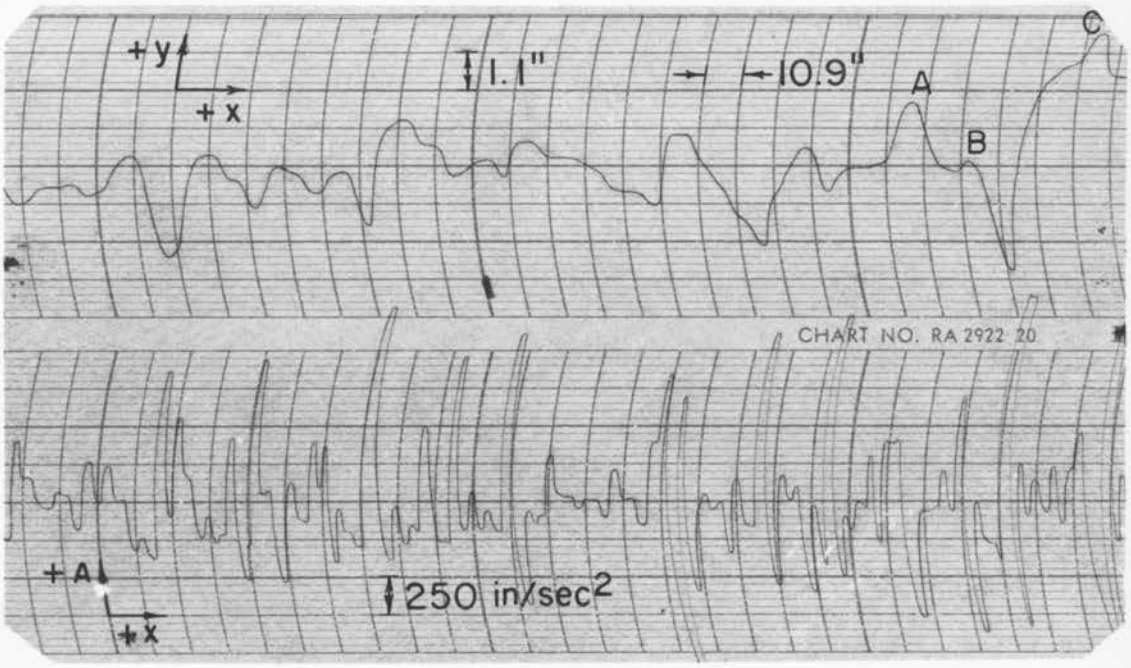
+y
+x
1.1"
10.9"
A
B
C
CHART NO. RA 2922 20
+A
+x
250 in/sec²

into its various frequency components and examine these separately. If the trace were available in electrical form, such as on magnetic tape from a tape recorder, this could easily be done. Electrical filtering could be used to remove all components except for those falling in the desired narrow frequency band.

In this study, the displacement signal was recorded on an oscillograph chart, and subsequently was not available in electrical form. Thus, an electrical filtering technique could not be used, and some other method of analysis had to be found.

A test track designer would be interested in the range of sizes of obstructions found in the field, and in the spacing of these obstructions. He would then know whether his test track design corresponded to mild, moderate or severe field conditions. Consequently, the non-row crop data charts were analyzed with the objective of determining size and spacing distribution for field obstructions.

Before the spacing of obstructions can be measured, an obstruction must be defined. Consider the peaks labeled A, B and C in Figure 17. If peak B constitutes an obstruction, the horizontal distance from A to C is broken up into two spaces. If peak B does not constitute an obstruction, the distance from A to C is only one space. For purposes of analysis, a peak was called an obstruction if there existed

a depression of at least h_L chart lines between it and the next peak, where h_L takes on various values. Thus, in the initial analysis, the criterion would be that h_L must be greater than one chart line. Peak B would just meet this criterion and would be called an obstruction. Consequently, the horizontal distance from peak A to peak B would be recorded as eight chart lines. The horizontal distance from peak B to peak C would be recorded as sixteen chart lines. The remaining peaks on the chart would be subjected to the same criterion ($h_L > 1$ line) and the obstruction spacings would be recorded. The total number of spaces would be determined and subsequently, the percent of peak spacings of each length (i.e., 1, 2, 3, 4, · · · chart lines length) would be calculated. Finally, the percent of spacings greater than each length would be computed.

The whole process would then be repeated, this time with the criterion that h_L must be greater than two chart lines. In this analysis, the peak B in Figure 17 would not be considered an obstruction. The horizontal distance from peak A to peak B would be considered one space of 24 chart lines length. In subsequent analyses, h_L would be set at four lines, then six, ten, fourteen, twenty, twenty-five and thirty lines. In each analysis, a certain number of peaks would be eliminated from consideration, the minimum obstruction size would become greater, and the obstruction spacings would become

greater.

The above procedure was carried out for several non-row crop field surfaces. The results are tabulated in Tables 17 through 20, Appendix G. In these tables all length quantities have been converted from chart lines to inches. To make the conversion for each run, the vertical sensitivity was determined from the instrument attenuator settings. The horizontal sensitivity was determined from the event marker system, which left a mark on the chart once each wheel revolution. The chart length between event marks corresponds to the effective wheel circumference. The effective wheel circumference was determined as explained in Appendix E.

DISCUSSION AND RESULTS

Row Crop Fields

Three displacement traces are shown in Figure 18. These waveforms were all obtained in field number one, a corn field. The waveforms would not be expected to be identical, since the test tractor followed slightly different paths on the three runs. However, the similarity between the traces is evident. The trough-to-crest amplitude of these waves is approximately 2½ inches. In subsequent runs in a ridged soybean field, a similar result was obtained.

In all of the row crop fields, the soil was fairly uniform in consistency, and not cloddy. Under these soil conditions, the soil deformation caused by the bicycle tire was similar to that caused by the tractor tire. Thus, the accelerometer motion was not much different when the accelerometer was mounted on the bicycle wheel, as compared to when it was mounted on the tire feeler device.

Figure 18 also gives some indication of the action of the tire in transmitting motion. The natural frequencies of the test tractor were not measured. However, based on results obtained by Raney et al. (13) and Van Gerpen (17), the lowest natural frequency is at least 3 cps. On the other hand, while crossing 40-inch rows at 3 mph, the tractor had imposed a forcing function with a frequency of approximately 1.3 cps.

Figure 18. Displacement traces obtained in field number 1

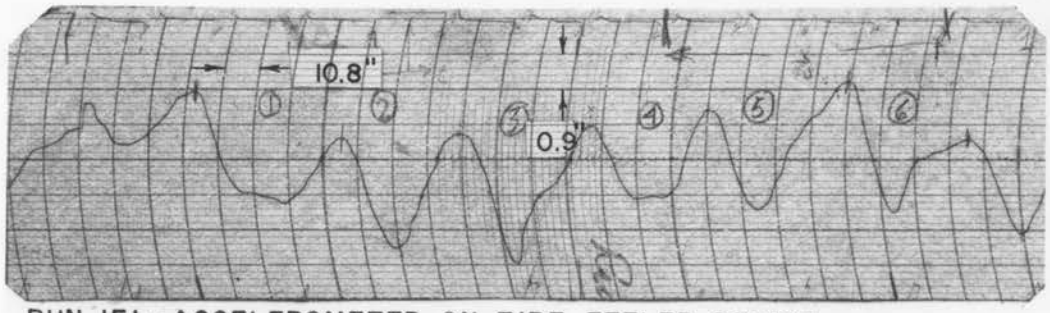

RUN IF1 - ACCELEROMETER ON TIRE FEELER DEVICE

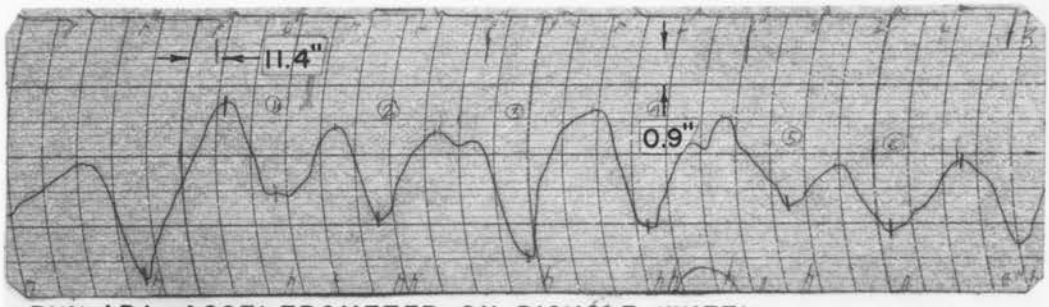

RUN IB1 - ACCELEROMETER ON BICYCLE WHEEL

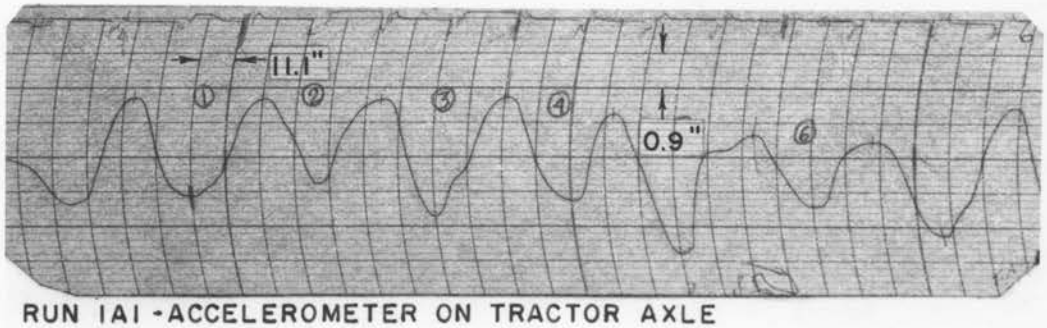

RUN IA1 - ACCELEROMETER ON TRACTOR AXLE

With the forcing frequency below the first natural frequency, the tire would be expected to magnify the motion induced by the field surface. The magnification factor would be expected to increase as the forcing frequency approached the natural frequency. For the runs made in this study, however, the frequencies were far enough apart to make the magnification factor nearly equal to one. Thus, the tire transmitted to the axle essentially the same motion imposed on the tire bottom by the field.

The results of roughness measurements in the row crop fields are given in Tables 5 through 16, Appendix F. The results obtained in Run 1F1 are typical, and are plotted in Figures 19, 20 and 21.

The top graph in Figure 19 shows the variation among the wavelengths. Although the field was planted and cultivated with 4-row equipment, no two sequential waves are identical in length. This indicates that the highest point in the effective profile is not always at the row center. The coefficient of variation, 23 percent, is not extremely large. Nevertheless, for exact simulation of corn row roughness on a test track, the wavelengths would have to be varied. This could be done by varying the spacing of bumps. If Raney's (13) system, i.e., programming a tractor mathematical model on an analog computer, was used in a vibration study, a wave generator would be used to simulate field roughness. In this case, some

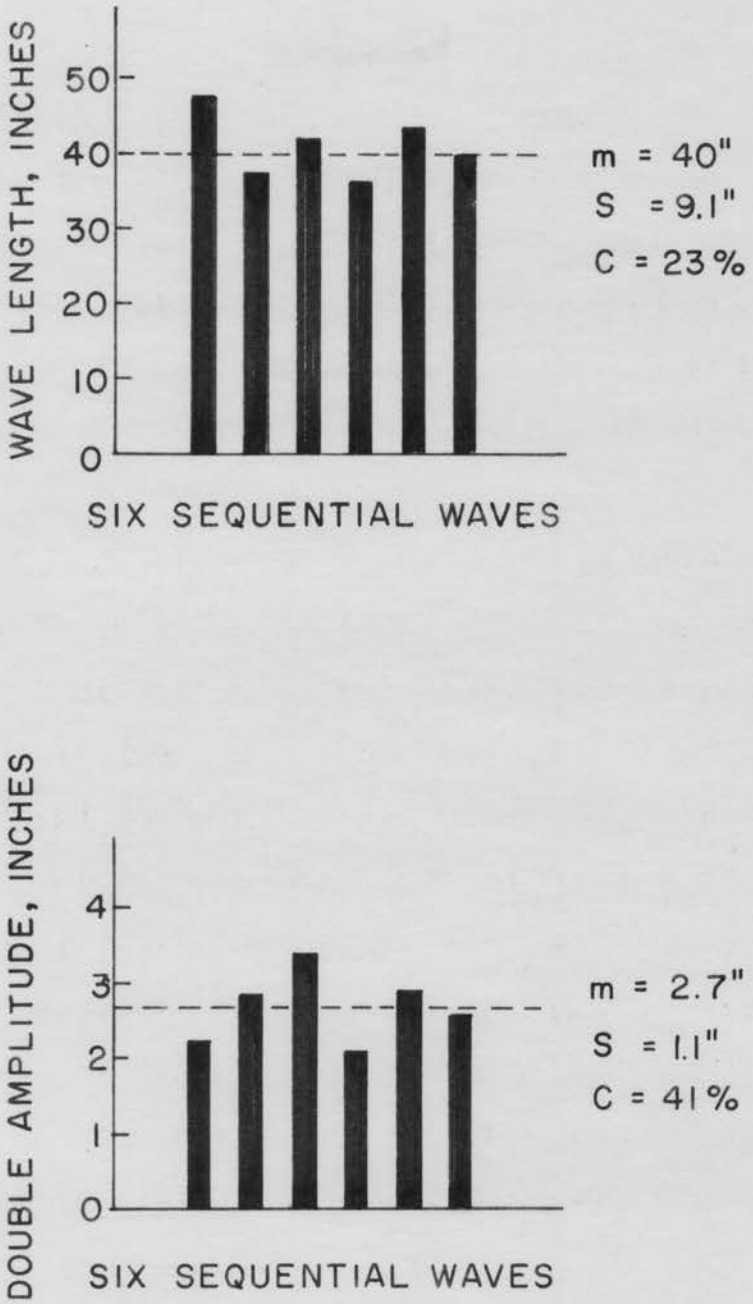

Figure 19. Comparison of six sequential waves in Run 1F1

provisions might be made for continually varying the frequency of the wave generator.

The bottom graph in Figure 19 is a typical comparison of double amplitudes of six sequential waves. There is a large variation among the double amplitudes, the coefficient of variation being 41 percent. Bumps of various heights would be required for exact simulation of this roughness on a test track. If the simulator was the wave generator mentioned above, provision would have to be made for continually varying the output amplitude of the wave generator.

The upper graph in Figure 20 illustrates the cosine coefficients obtained from the harmonic analyses of six sequential waves. Above each cosine harmonic number is shown a set of six bars. Each left-most bar represents the first wave on Run 1F1. The next bar to the right in each case represents the second wave, etc. Of particular interest in this graph is the dominance of the first cosine harmonic. The rapid tapering off of the higher harmonics is an indication of a relatively smooth waveform. The graph also indicates a fair amount of uniformity of first cosine harmonic content in the six waves. The higher harmonics are considerably more variable. The presence of the even numbered harmonics indicates a lack of half wave symmetry. That is, the wave troughs are not symmetrical to the crests.

The sine coefficients are shown in the lower graph of

Figure 20. Comparison of results of harmonic analyses on six sequential waves in Run 1F1

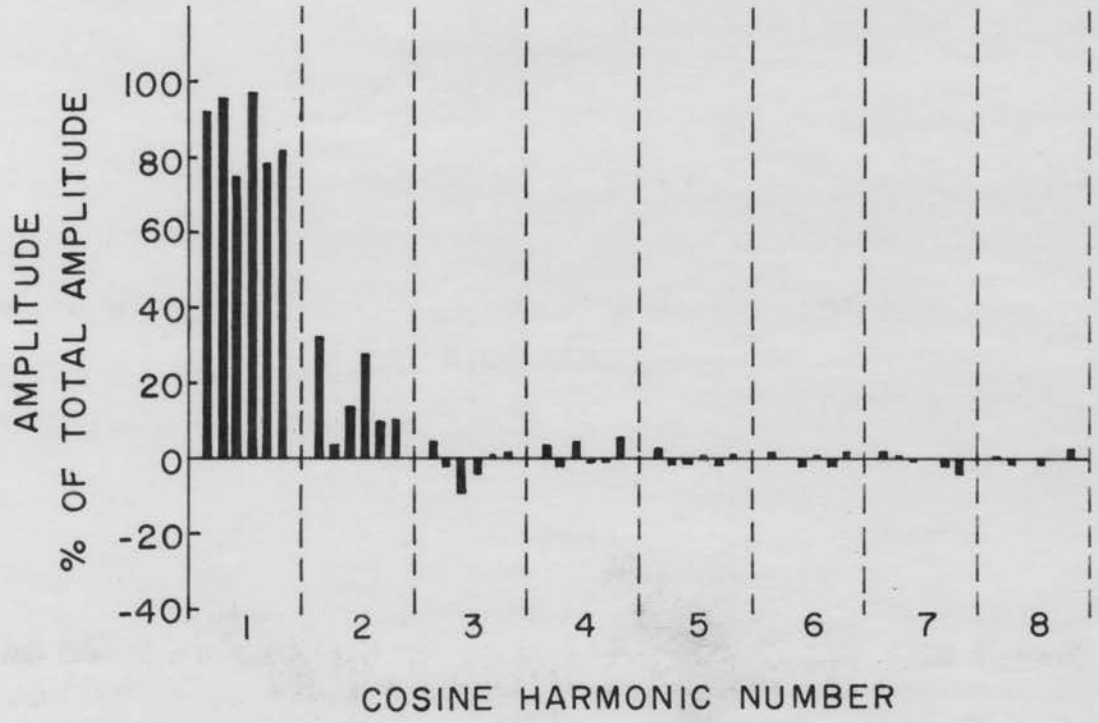
AMPLITUDE
% OF TOTAL AMPLITUDE
100
80
60
40
20
0
-20
-40
1
2
3
4
5
6
7
8
COSINE HARMONIC NUMBER

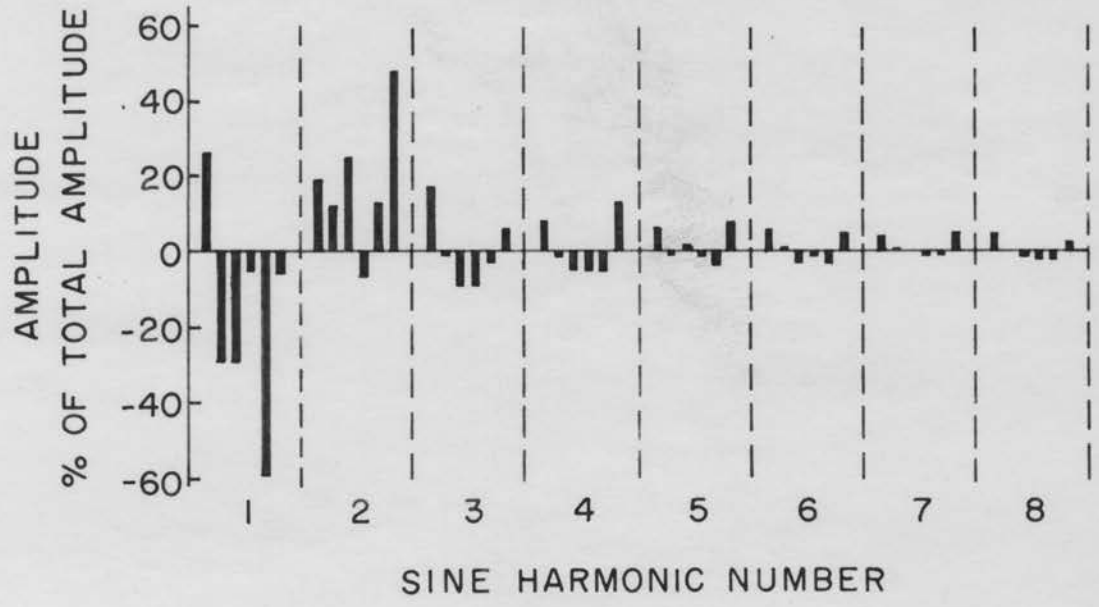
AMPLITUDE
% OF TOTAL AMPLITUDE
60
40
20
0
-20
-40
-60
1
2
3
4
5
6
7
8
SINE HARMONIC NUMBER

Figure 20. The sine harmonics are generally more variable than the cosine harmonics. The presence of the sine harmonics indicates another lack of symmetry. In particular, there is no vertical axis of symmetry.

Figure 21 is a comparison of the constant terms obtained from the harmonic analyses. The minimum constant term was considered to be zero. Thus, the graph indicates differences in average heights of the waves. The variation is rather large, considering that the average double amplitude of this set of waves is only 2.7 inches.

From the preceding discussion, it is apparent that exact simulation of the effective surface profile of row crop fields would be quite difficult. Figure 22 illustrates an attempt to mathematically approximate a corn field effective surface. The equation given with the lower pair of waves is based upon the average first and second cosine harmonic contributions, average first and second sine harmonic contributions, average constant term, and average wavelength of the six sequential waves from Run 1F1. There is a reasonably good fit between the mathematical waveform and the waveform actually measured. However, the closeness of the upper pair of waves shows that the fit is nearly as good using only the first cosine harmonic.

Throughout this thesis, there has been frequent reference to effective field surfaces. The oscillograph traces obtained are obviously lines, not surfaces. However, an

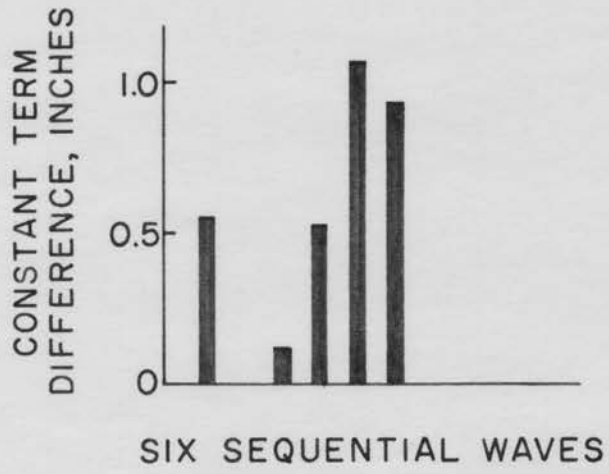

Figure 21. Differences among the constant terms of six sequential waves in Run 1F1

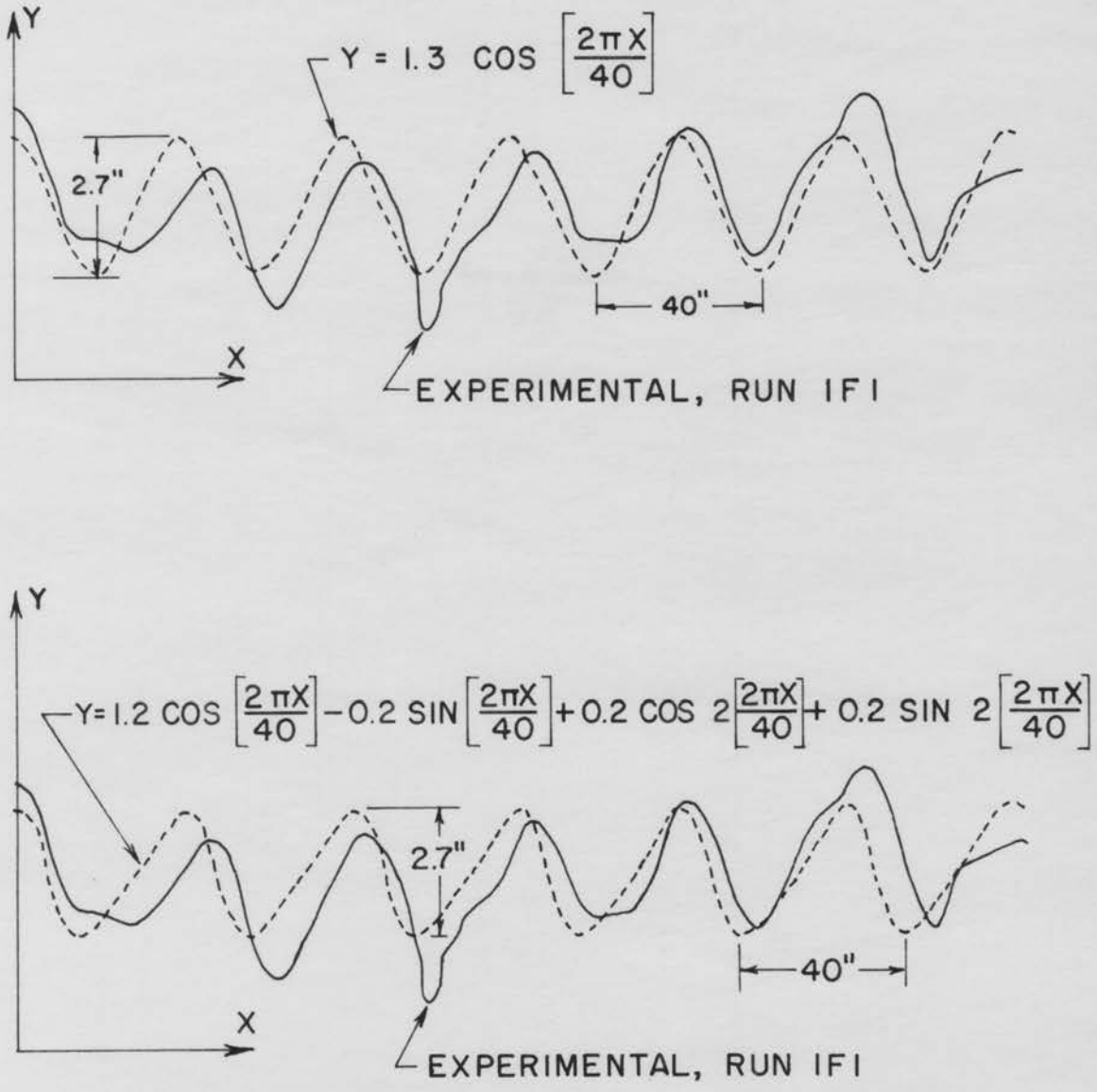

Figure 22. Mathematical approximations to the effective profile measured in Run 1F1

oscillograph trace can be thought of as the edge view of a surface which extends back into the paper. This conception would be fairly realistic for traces obtained in a corn field when the test tractor was traveling perpendicular to the row direction. As a matter of fact, all of the waves analyzed were obtained when the tractor was moving essentially perpendicular to the row direction. For convenience, the plane in which these waves lie will be designated as the perpendicular cross section, i.e., perpendicular to the row direction. In representing one of these waves with a Fourier trigonometric series, the wavelength L would be the horizontal distance from one peak to the next, measured in the perpendicular cross section. If the tractor travels across the rows making an angle β with the row direction, the above-mentioned Fourier series must have one modification before it can represent the resulting wave shape. The wave length L must be replaced by a new wavelength L', where:

$$L' = \frac{L}{\sin \beta} .$$

If the tractor direction of travel across a periodic surface is not perpendicular to the row direction, the wave shapes are merely "stretched out" versions of the wave shapes obtained when the tractor is traveling perpendicular to the row direction. This is because the sine and cosine coefficients of the Fourier series representing the periodic

surface are independent of the wave length. This fact can be deduced from the coefficient formulas, which are rewritten below:

$$a_n = \frac{2}{N} \sum_{K=0}^{K=N-1} y_K \sin n\left(\frac{2\pi K}{N}\right) \tag{4}$$

$$b_n = \frac{2}{N} \sum_{K=0}^{K=N-1} y_K \cos n\left(\frac{2\pi K}{N}\right). \tag{5}$$

N is the number of equal intervals into which the wavelength is divided, where N can be arbitrarily large. There is no term in the formulas to represent the length of these equal intervals. Hence, the coefficients are independent of the interval length and consequently, are independent of the wavelength.

All of the row crop fields except field 3 were worked with 4-row equipment which was set for 40-inch rows. The coefficients of variation among wavelengths for these fields ranged from 9 percent to 23 percent. The ridges in field 3 were formed with an experimental 1-row machine. A great deal of variation in row spacing resulted. This was reflected in a high coefficient of variation among wavelengths for field 3. This coefficient was 41 percent, as shown in Table 11, Appendix F.

Non-Row Crop Fields

Three displacement traces from field 4 are compared in Figure 23. Field 4 was a relatively rough plowed field. The

Figure 23. Displacement traces obtained in field number 4

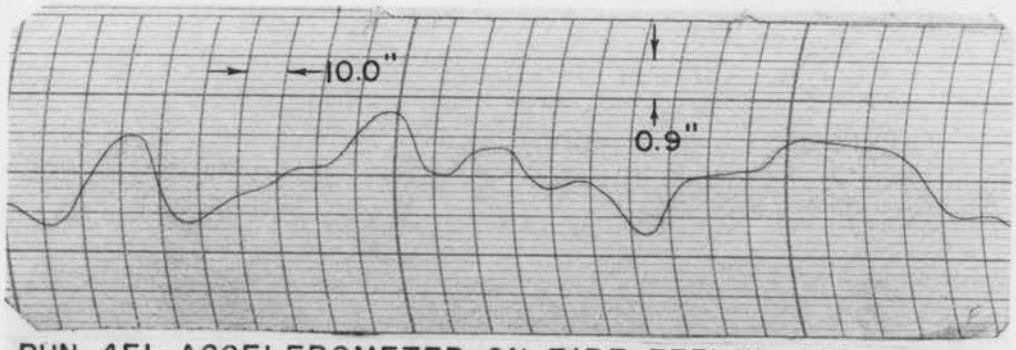

RUN 4FI-ACCELEROMETER ON TIRE FEELER DEVICE

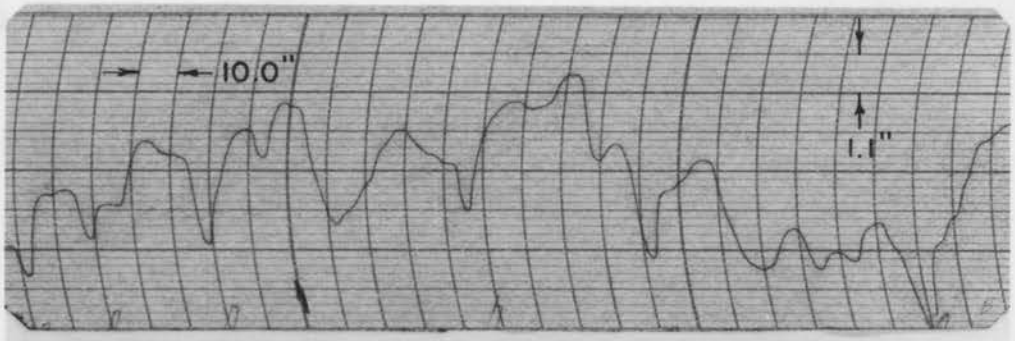

RUN 4BI-ACCELEROMETER ON BICYCLE WHEEL

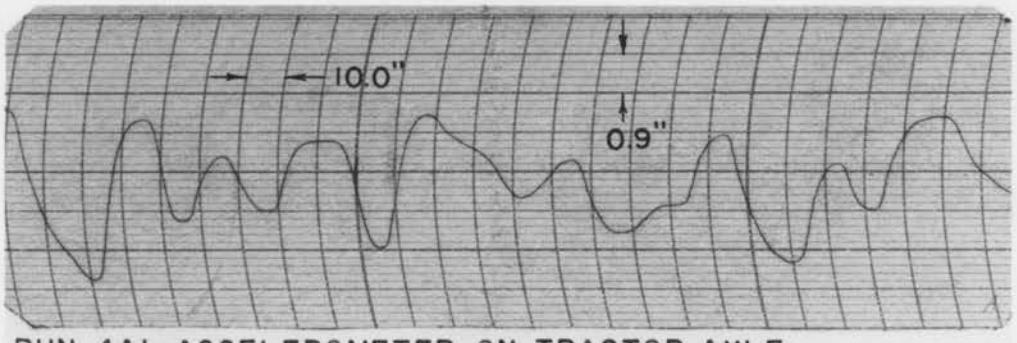

RUN 4AI-ACCELEROMETER ON TRACTOR AXLE

surface was made up of hard earth clumps and clods randomly arranged. From Figure 23, it is obvious that the accelerometer was subjected to a much rougher ride on the bicycle wheel than when it was mounted on the tire feeler device. The vertical movements were greater and occurred with much greater frequency. This unsatisfactory performance of the bicycle wheel in a plowed field contrasts with its performance in a corn field (Figure 13), where the bicycle wheel did trace out the desired surface profile. There is a logical explanation for this situation. The bicycle wheel was designed to have essentially the same unit contact pressure as the front tractor tire. However, the total wheel loads were considerably different. The total bicycle wheel reaction was 160 pounds, while the tractor wheel reaction was 885 pounds. In the corn fields, where the soil was of uniform consistency, the soil deformation depended on the unit pressure applied, not total load. In the plowed fields, the hard earth clumps had to support a wheel, be pressed down into the underlying soil, or be crushed. The bicycle wheel was unable to apply sufficient total force to depress or crush the earth clumps. Thus, the bicycle wheel had to ride over a highly irregular surface. The tractor tire, being able to apply much greater total force, was able to depress or crush many of the clumps and thereby create a smoother path.

Figure 23 also illustrates the motion of the tractor

front axle as compared to the tire-bottom motion. The frequency of oscillation is greater for the axle. This implies that the tractor natural frequencies are being excited, and that the tractor tire is constantly flexing.

The preceding discussion indicates that, for the plowed fields, the effective surface profiles were not obtained when the accelerometer was mounted on the bicycle wheel or on the tractor axle. Consequently, the only runs analyzed for these fields were those where the accelerometer was mounted on the tire feeler device. The results are tabulated in Tables 17 through 20, Appendix I, and are plotted in Figures 24 through 27. In these graphs, the steepness of the curves is an indication of the concentration of obstruction spacings of a particular length. The steeper the curve, the greater is the concentration of obstruction spacings of that particular length.

The data for Figure 24 were obtained in field 4. This field was very rough due to wet plowing. It can be seen that virtually all obstruction spacings were greater than 20 inches. The third and fourth curves blend together, indicating that very few obstructions had minimum heights in the range 0.72 to 1.09 inches. The wide spacing between the fourth and fifth curves indicates that many obstructions had a minimum height in the range 1.09 to 1.81 inches. The greatest minimum obstruction height found was 4.53 inches.

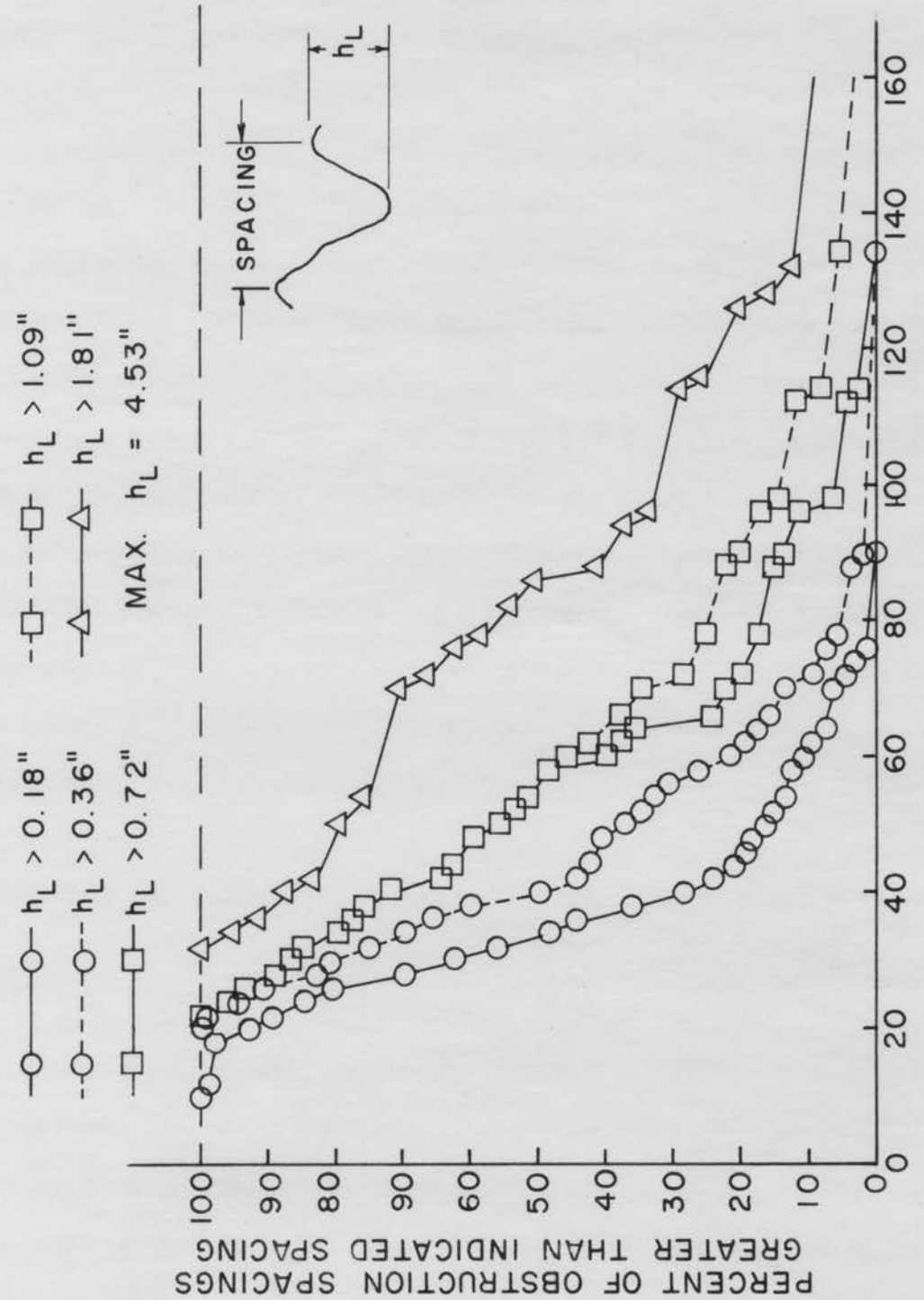

Figure 24. Distribution of obstructions encountered in Run 4F1, with tractor speed of 2.8 mph

Figure 25 is based on results obtained in field 5. This field was a plowed field that had been allowed to fallow during the summer and, consequently, the surface was only moderately rough. Although the tractor throttle setting was identical in fields 4 and 5, the tractor had greater speed in field 5 due to decreased roughness. Again in this field, there were very few obstruction spacings less than 20 inches.

The data for Figure 26 were recorded in field 7, a meadow. The tractor speed was 3.3 mph, again with the same throttle setting as in the plowed fields. The data for Figure 27 were recorded in the same meadow, but with the tractor transmission in a higher gear. The graphs indicate not much difference in obstruction distributions at the two speeds, or in greatest obstruction heights. Evidently the tractor tire was able to maintain ground contact, even at the higher speed. In this meadow--as in the plowed fields--obstruction spacings less than 20 inches were rare.

Re-evaluation of Measuring Techniques

The accelerometer proved to be a suitable basic motion measuring device. However, the acceleration trace alone was of little value in providing a picture of a field surface. This is evident in Figure 17, where an acceleration trace is shown. Each time the displacement trace goes through an inflection point, the acceleration must be zero. The resulting jagged-

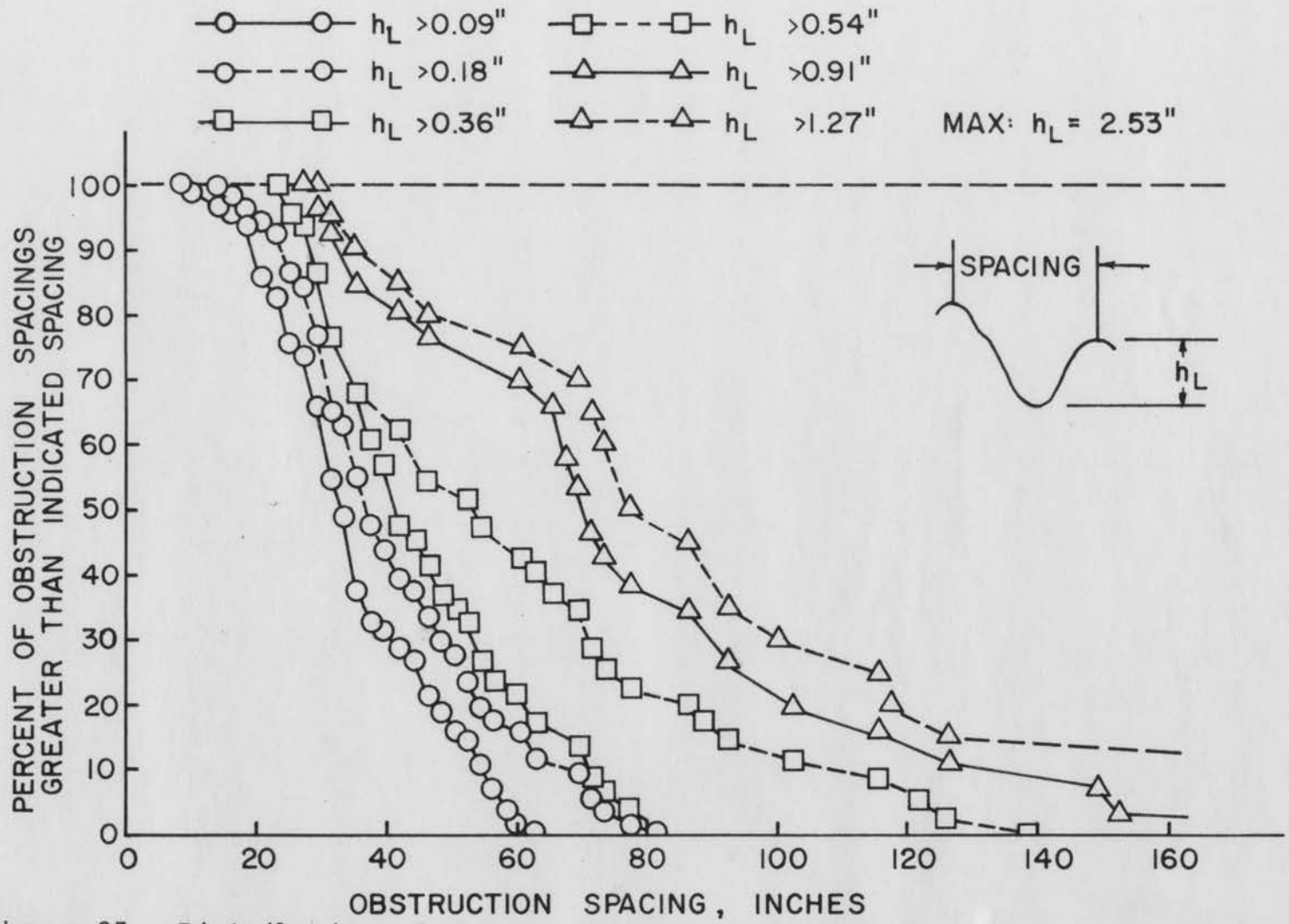

Figure 25. Distribution of obstructions encountered in Run 5F1 with tractor speed of 3.0 mph

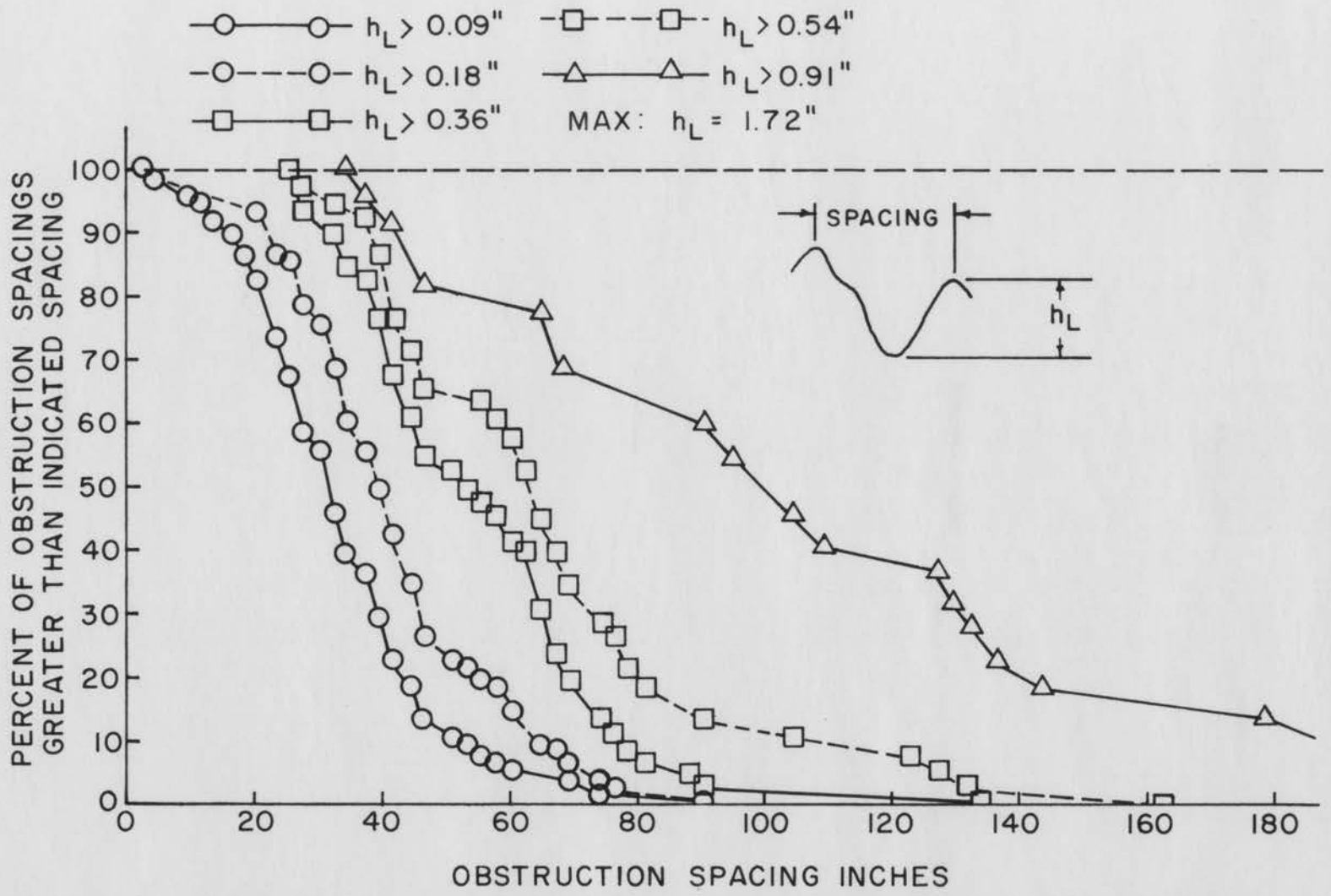

Figure 26. Distribution of obstructions encountered in Run 7F1 with tractor speed of 3.3 mph

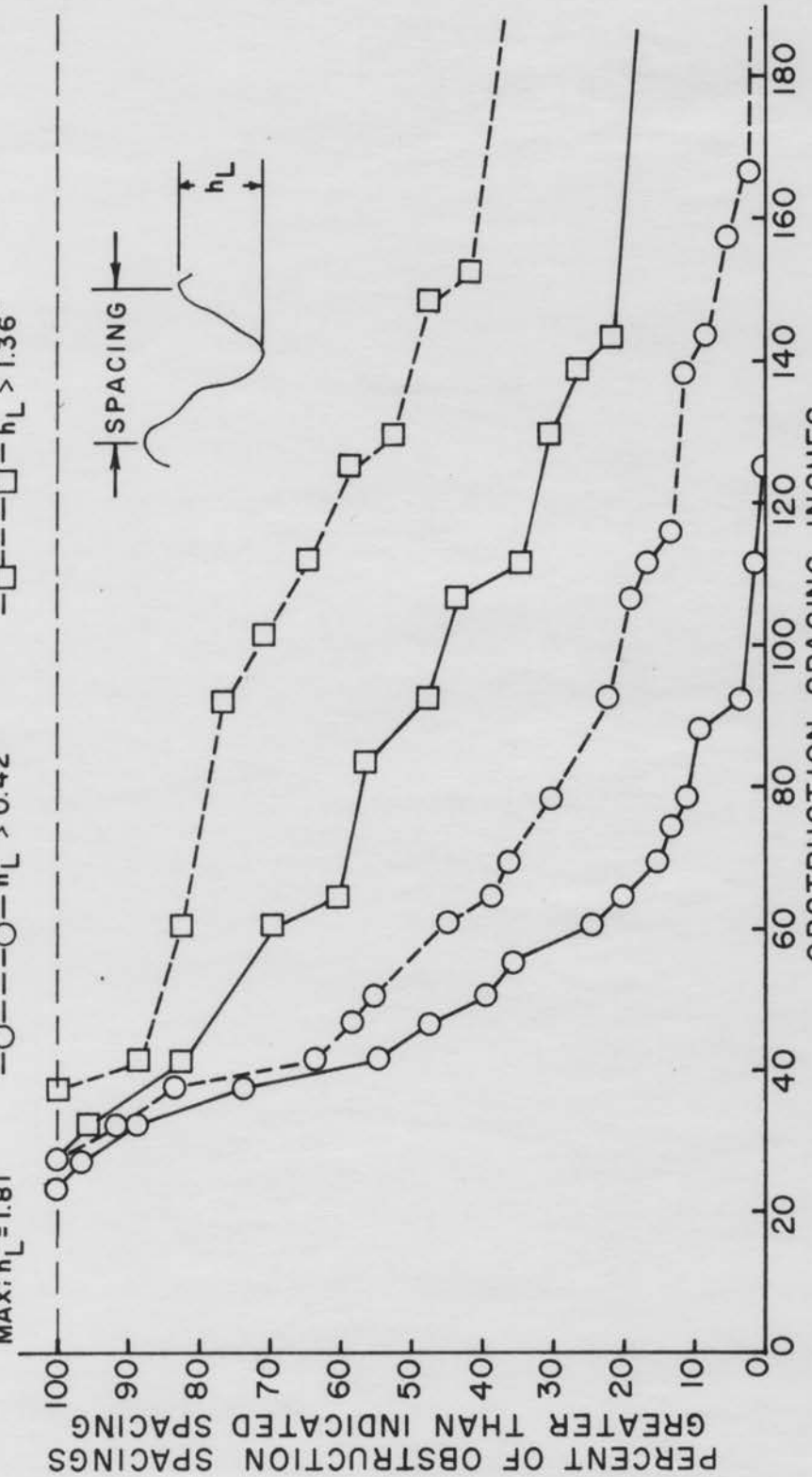

Figure 27. Distribution of obstructions encountered in Run 7F2 with tractor speed of 6.6 mph

ness of the acceleration trace makes any kind of planimetering extremely difficult. Thus, integrating circuits are a virtual necessity in this type of work. The limited low frequency response of R-C circuit integrators then becomes a problem. As previously mentioned, a tractor crossing 40-inch corn rows at 3 mph has imposed a forcing function of approximately 1.3 cps frequency. Equally low frequencies are encountered in non-row crop fields. Thus, integrators for this work should be accurate to 1 cps or lower.

If a double-integrator is designed for integrating 1 cps signals, its high frequency response is severely limited by decreasing signal magnitude. For each doubling of the frequency of a constant amplitude input signal, the double-integrator output is divided by 4. Thus, if the output signal of a double-integrator is of suitable size at 1 cps, it is only one-fourth as large at 2 cps and only 1/16 as large at 4 cps. The difficulty can be overcome if a calibrated attenuator is available between the double-integrator and the recording device. In this case, the integrator output is amplified to a suitable magnitude for recording at the highest frequency desired. For low frequency work, the attenuator is then used to reduce the signal to manageable size.

Blocking capacitors are a necessity when integrators are used in this type of work. The blocking capacitors must remove DC signals arising from persistent accelerometer mis-

alignment in the gravity field, as well as DC signals from amplifier drift. Otherwise, the integrators would receive a signal corresponding to constant acceleration, and the displacement recorder would quickly be driven off scale.

In this study, effective surface profiles were recorded on oscillograph charts. For quick visual scanning of the results, this method of recording is good. For detailed analysis, there is a great advantage in recording the displacement trace in such a way that it can be reconverted into electrical form. Recording on magnetic tapes would be a suitable method. A very low frequency tape recorder would be required for this work. Such recorders are available. For example, Crandall et al. (2, p. 176) point out that tape recorders used to record aircraft gust and ocean wave data may encounter frequency components as low as 0.01 cps.

The only piece of apparatus which gave consistently reasonable results was the tire feeler device. This device also has limitations. In spite of the fact that efforts were made to reduce drag, the tire feelers did retard the wheel rotation (See Appendix E). The problem was not solved by replacing the feeler rods with rollers. This was tried, but the rollers quickly became blocked with dirt and stopped rotating. The tire feeler device was also unsuitable where wheel sinkage was excessive. Under these conditions, soil would pile up around the feeler supporting framework and subsequently force

the feelers up onto the sides of the tire. Proper streamlining of the supporting framework should reduce this problem.

Simulation Techniques

The purpose of field roughness data is to aid in the intelligent design of roughness simulators. The simplest type of roughness simulator is a test track on which obstructions are placed. Field roughness studies are an aid to determining realistic sizes, shapes and spacing of bumps to place on the track. A similar statement holds if the simulator is a treadmill instead of a track.

Using the above-mentioned simulators, a tractor prototype would be required for comfort testing. Raney et al. (13) have introduced the concept of pre-prototype design screening by use of an analog computer. Raney has written a mathematical model to describe the vibration of a tractor. The model can be programmed on an analog computer. Since tractor parameters are represented by appropriate variable circuit parameters, the simulated tractor parameters can be changed readily. The forcing functions applied to the computer circuits are analogous to field roughness. Hence, field roughness studies are an aid to determining realistic forcing functions. For example, to simulate the vibration of a tractor crossing corn rows, a cosine wave or a combination of sine and cosine waves might be applied to the computer circuits.

Alternately, if magnetic tape records of the field roughness were available, tape recorder-playback could be used to supply the forcing functions to the analog computer.

Finally, field roughness can be simulated by placing the tractor on a shake table. A wave generator or magnetic tape recorder can serve as the input, or certain motions can be generated by means of cams. The tractors which can be tested on a shake table are limited in size. Consequently, either a test track or a treadmill furnish a more suitable means for comfort testing prototypes of farm tractors.

The results obtained in this study are valid for a particular set of circumstances, and are not presumed to represent field conditions in general. The primary purpose of this project was to develop a means for measuring effective field surface roughness, and not to investigate all of the factors involved. More studies will be required to evaluate other factors before sufficient published data are available for the realistic design of field roughness simulators. For example, no attempt was made to study motion inputs to a tractor rear tire. Also, a wider range of field conditions should be investigated.

SUMMARY AND CONCLUSIONS

In recent years, there has been increasing concern about the effect of tractor vibration on the tractor operator. Because of this concern, there is a trend toward designs aimed at reducing the vibration which reaches the tractor operator. These designs require testing on standardized roughness simulators. Unfortunately, no published field roughness data are available as guides for designing realistic roughness simulators.

The purpose of this experiment was to develop and apply a means for determining the effective roughness of field surfaces. For deformable field surfaces, the shape of the effective surface depends upon characteristics of the vehicle crossing the surface. Thus, simplifying assumptions had to be made about the vehicle. The vehicle was considered to be a vibrating system, with the motion inputs to the tire bottoms constituting forcing functions. Since in the field these motion inputs are generated by effective field roughness, the effective roughness "seen" by a tire could be measured by measuring the motion input to that tire. An Allis-Chalmers D-17 Utility tractor was used in the study, and motion inputs to the right front tire were measured.

An accelerometer was used for motion detection. High frequency acceleration signals were attenuated by electrical filtering. Two electric integrators were constructed for

converting the acceleration signal to a displacement signal. Acceleration and displacement traces were recorded side by side on a 2-channel oscillograph.

A tire feeler device, on which the accelerometer could be mounted, was constructed for following the motion of the tractor tire bottom. Where tractor wheel sinkage was excessive, it was difficult to keep the feeler device in place. Consequently, a spring loaded bicycle wheel was also constructed in an attempt to measure effective surface roughness. The wheel diameter and the unit contact pressure for the bicycle wheel were similar to those for the tractor wheel. A means was also provided for measuring motion of the tractor front axle at the wheel center.

In the field, the electronic instruments were kept in a trailer. The test tractor was driven around this trailer on an 80-foot-radius, circular path. Suitable cables were provided for interconnecting the electronic instruments to the accelerometer on the tractor.

Roughness measurements were made in row crop fields and in non-row crop fields. Fourier harmonic analyses were applied to the waveforms obtained in row crop fields. A digital computer was used to evaluate the coefficients in the Fourier series. For the non-row crop fields, a study was made of the size and spacing distribution of obstructions.

The following conclusions are drawn from the results of

this study:

1. It is possible to measure effective field surface roughness. An accelerometer can be used for the motion detection, provided that suitable integrators are also used. It is not possible to visualize the surface profile from the acceleration trace alone.

2. Similarity of wheel diameter and unit contact pressure of two wheels is not enough to insure that they will receive the same forcing function from a given deformable surface. Total wheel load is also important.

3. Motion inputs from the field cannot be measured at the tractor axle, since excitation of the tractor natural frequencies greatly influences the axle motion.

4. In this study, the effective trough-to-crest row heights encountered ranged from 1.3 inches to 3.7 inches, while the average was 2.4 inches. The surface profile had a complete lack of symmetry and deviated from periodicity. However, these surface profiles could be approximated by mathematical waveforms.

5. In the non-row crop fields, obstruction spacings less than 20 inches were rare. The greatest effective trough-to-crest height found was 4½ inches. The oscillograph trace was of limited value in analyzing these non-row crop field surfaces, since electrical filtering could not be used in analyzing the trace.

SUGGESTIONS FOR FURTHER STUDY

The author suggests the following topics for further research regarding farm equipment operator comfort:

1. A study of the effect of certain tractor variables upon the shape of effective surface profiles. These variables should include tractor weight, speed, and wheel diameter.

2. The development of nonlinear differential equations to describe the vibration of a tractor when the forcing functions have large amplitudes.

3. A study to determine noise levels on and around farm equipment.

LITERATURE CITED

1. Coerman, R., Ziegenruecker, G., Wittwer, A. L., and Von Gierke, H. E. The passive dynamic mechanical properties of the human thorax-abdomen system and of the whole body system. Aerospace Medicine 31:443-445. 1960.

2. Crandall, S. H., Dyer, I., Mains, R. M., McClintock, F. A., Metzgar, K. J., Pian, T. H., Poritsky, H., Powell, A., Priest, D. E., Rona, T. P., and Siebert, W. M. Random vibration. New York, N. Y. John Wiley and Sons, Inc. [c1958].

3. Den Hartog, J. P. Mechanical vibrations. 2nd ed. New York, N. Y. McGraw-Hill Book Co., Inc. 1940.

4. Dupuis, H. Schwingungsuntersuchunger bei Schleppern auf einem Rollenprufstand. Landtechnische Forschung 10: 145-156. 1960.

5. Haack, M. Human tolerance to vibrations in farm machines. Agricultural Engineering 37:253-257. 1956.

6. Hornick, R. J. Effects of tractor vibration on operators. Agricultural Engineering 42:674-675, 696-697. 1961.

7. Jacklin, H. M. and Liddell, G. J. Riding comfort analysis. Purdue University Engr. Exp. Sta. Res. Series Bull. 44. 1933.

8. Janeway, R. N. Passenger vibration limits. Society of Automotive Engineers Journal 56:48. 1948.

9. Loeb, M. A further investigation of the influence of whole-body vibration and noise on tremor and visual acuity. U. S. Army Medical Research Laboratory Report 165. 1955.

10. Mitchell, F. H. Fundamentals of electronics. Cambridge, Mass. Addison-Wesley Publishing Co., Inc. 1955.

11. Morrison, C. S. and Harrington, R. E. Tractor seating for operator comfort. Paper presented at the American Society of Agricultural Engineers Annual Meeting, Iowa State University of Science and Technology, Ames, Iowa, June 25-28, 1961. (Mimeographed) Moline, Illinois. Product Development Department, Deere and Company. 1961.

12. Postlethwaite, F. Human susceptibility to vibration. Engineering 157:61-63. 1944.

13. Raney, J. P., Liljedal, J. B., and Cohen, R. The dynamic behavior of farm tractors. American Society of Agricultural Engineers Transactions 4:215-218, 221. 1961.

14. Roesegger, R. and Roesegger, S. Health effects of tractor driving. Journal of Agricultural Engineering Research 5:241-275. 1960.

15. Roman, J. A., Coerman, R., and Ziegenrucker, G. Vibration buffeting and impact research. Aerospace Medicine 30:118-125. 1959.

16. Thomson, W. T. Mechanical vibrations. 2nd ed. New York, N. Y. Prentice-Hall, Inc. 1954.

17. Van Gerpen, H. W. Evaluating tractor seating comfort. Agricultural Engineering 37:673-676. 1956.

18. Vandenberg, G. E., Cooper, A. W., Erickson, A. E., and Carleton, W. M. Soil pressure distribution under tractor and implement traffic. Agricultural Engineering 38:854-855, 858-859. 1957.

19. Zeller, W. Masseinheiten für Schwingungsstärke und Schwingungs-empfindungsstarke. Automobile Technische Zeitschrift 51:95-97. 1949.

ACKNOWLEDGMENTS

The author is grateful to Dr. C. W. Bockhop for his counseling, assistance and encouragement throughout the research project and the writing of this thesis.

Thanks are also due to Professor Beresford, Professor Chamberlin, Dr. Charity and Dr. Davis for serving on the graduate committee.

The author thanks the Department of Agricultural Engineering for providing equipment and facilities.

The author is also grateful to his wife, Carol Ann, for her encouragement and understanding throughout the graduate program.

APPENDIX A: ACCELEROMETER CALIBRATION

Initial Balancing

The procedure to be followed in calibrating an accelerometer depends upon whether the accelerations to be measured are in a vertical or horizontal direction. If they are in a vertical direction, one must consider the static deflection of the accelerometer springs resulting from the pull of gravity on the seismic mass. It is necessary for the accelerometer output voltage to be zero after this static deflection has occurred. Then the acceleration reading will be zero with the accelerometer resting motionless and with its sensitivity axis vertical. In brief, zero signal voltage should correspond to the equilibrium position of the seismic mass when the accelerometer is motionless and its axis of sensitivity is vertical. If the signal voltage is not zero under these conditions, it can be forced to zero by using balancing controls to balance the wheatstone bridge within the accelerometer. In fact, this balancing is always done initially.

Static Method

For static calibration, the accelerometer was initially balanced with its base resting on a leveled surface, so that the sensitivity axis was vertical. Next the accelerometer was

rotated 90° so that the sensitivity axis was perpendicular to the pull of gravity. The resulting output signal was assumed to correspond to 1 g of acceleration. As verified by the Iowa State Physics Department, 1 g at Ames corresponds to 980.28 cm/sec^2, or 386 in/sec^2. Therefore, the amplifier gain was adjusted for 7.72 lines oscillograph pen deflection. This gave a sensitivity of 50 in/sec^2 per line at attenuator 10. One entry was made in Table 1 and one point was plotted on Figure 28. This completed the calibration. To check linearity, the accelerometer was also oriented with θ (defined in Figure 28) set at 45°, 135°, and 180°. The resulting accelerometer responses were entered in Table 1 and Figure 28. The accelerometer output, v, should have been

$$v = 7.72\ (1 - \cos\theta) \qquad \text{for } 0° \leq \theta \leq 180°.$$

However, Figure 28 shows that the output deviated from the theoretical output. Also, the maximum acceleration attainable by this static method was $2g(\theta = 180°)$. Therefore, provision was made for checking the accelerometer dynamically.

Semi-Dynamic Method

For dynamic methods of calibration a centrifuge can be used. The rear wheel of an ordinary farm tractor seemed suitable for a centrifuge. A Case 830 tractor was used. Blocks were used under the rear axle to keep the rear wheels free of the floor. The rear axle was carefully leveled. Figure 4 is a photograph of the calibration apparatus.

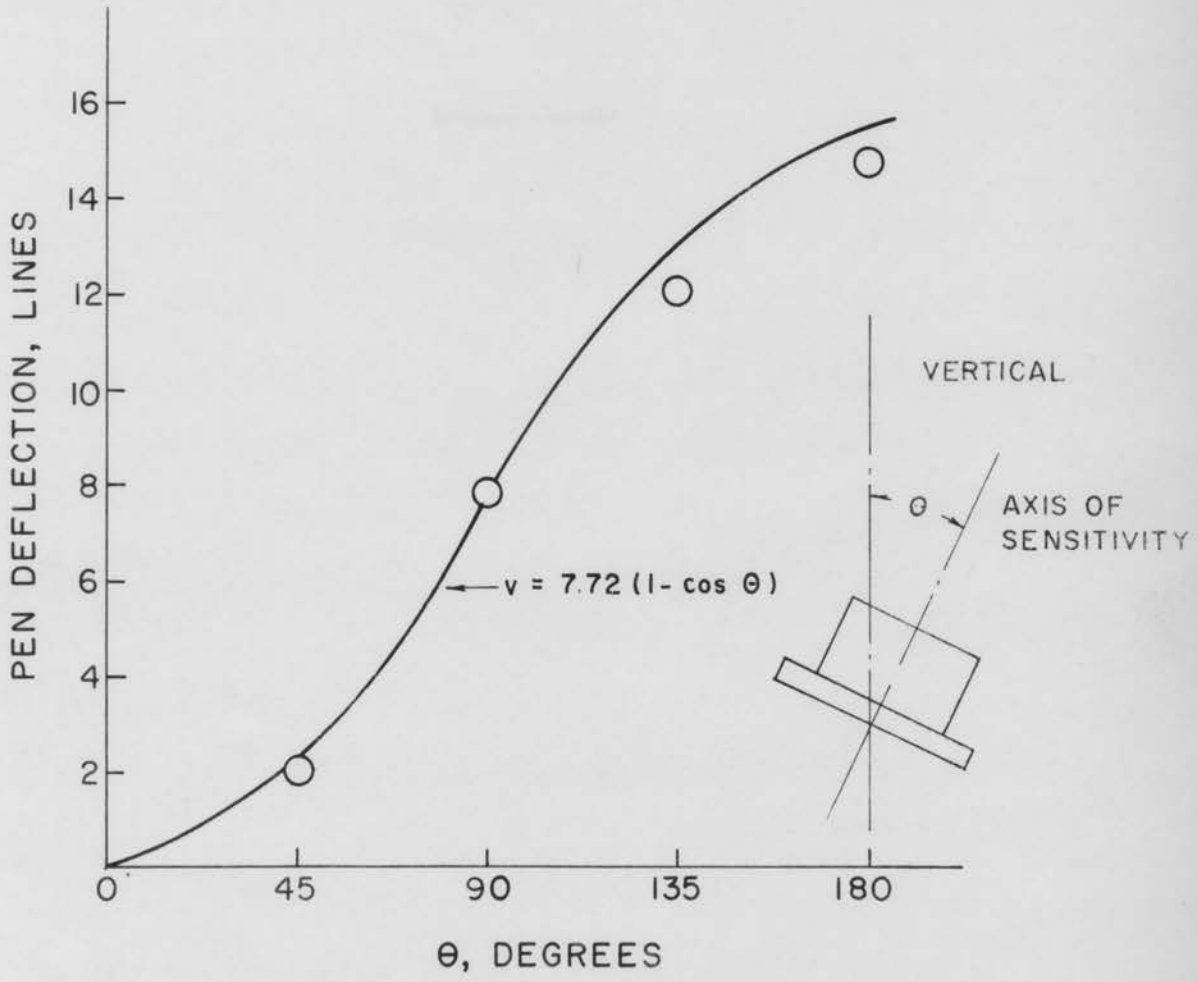

Figure 28. Results of static accelerometer calibration with a static linearity check

Table 1. Results of static accelerometer calibration with a static linearity check

θ, degrees	Theoretical apparent acceleration, g's	Theoretical pen deflection, lines	Actual[a] pen deflection, lines
0	0.00	0.00	0.0
45	0.29	2.26	2.0
90	1.00	7.72	7.0
135	1.71	13.18	12.1
180	2.00	15.44	14.7

[a]Attenuator on acceleration amplifier set at 10.

The left rear wheel brake was locked, and the accelerometer mounted on the right rear wheel. The accelerometer was oriented so that its axis of sensitivity was perpendicular to and intersecting with the center line of the rear axle. The center of the accelerometer was 13.5 inches from the rear axle center line. The base of the accelerometer faced away from the wheel center. This particular orientation of the accelerometer was suitable for measuring normal acceleration of the wheel.

The four leads to the accelerometer bridge were taken from the rotating wheel through a four-channel mercury slip ring assembly to the recording instruments. Not enough channels were available for the leads to the accelerometer heater. Consequently, the heater was operated only between calibration runs, and the heater leads were disconnected for the short

duration of the runs. The transformer in Figure 4 was used to reduce 115 volt AC current to the 28 volts required by the heater.

The mercury slip ring assembly incorporated a cam and breaker point assembly. The cam was designed to open the contact points once per axle revolution. This feature was used in conjunction with the oscillograph event marker to give one reference mark for each wheel revolution. Therefore, knowing the oscillograph chart speed it was possible to calculate the wheel rotational speed during any revolution.

The accelerometer was initially balanced with its sensitivity axis vertical. Consequently, the oscillograph pen deflection during calibration runs was a measure of normal acceleration only with the accelerometer at BDC (bottom dead center) on the wheel. At any other time the effect of gravity modified the accelerometer response. As the accelerometer moved from BDC to TDC (top dead center), and vice versa, the oscillograph pen deflected a distance corresponding to 2 g of acceleration.

After initial balancing, the tractor wheel was rotated until the accelerometer sensitivity axis was horizontal. In this position, the accelerometer output was assumed to correspond to 1 g of acceleration. The amplifier gain was set to give a 7.72 lines deflection with the attenuator at 10. As in the static tests, this corresponded to a sensitivity of 50

inches/sec^2 per line at attenuator 10.

As is evident from Figure 29, three separate acceleration records were available after each run. The first was normal acceleration, calculated from the wheel speed and the radius length to the accelerometer. For this calculation, the equation used was:

$$A_n = r\omega^2 = 13.5 \left[\frac{2\pi\gamma}{\delta}\right]^2$$

where A_n = normal acceleration, in/sec^2

r = radius to accelerometer = 13.5 inches

γ = oscillograph chart speed, mm/sec

δ = distance between event marks, mm

ω = angular wheel velocity, rad/sec.

The second acceleration record was the acceleration measured by the accelerometer at BDC on the wheel. The third acceleration record was the 2 g variation due to the accelerometer rotation in the gravity field.

For each run, the number of lines pen deflection from the BDC peaks to the TDC peaks was divided into 772 inches/sec^2 to obtain a dynamic sensitivity in in/sec^2 per line. When this dynamic sensitivity for each run was multiplied by the lines deflection at BDC, an estimate of accelerometer acceleration at BDC resulted.

The resulting data are tabulated in Table 2. The accelerations below 900 inches/sec^2 are also plotted in Figure 30. Perfect agreement between recorded and centrifuge

Figure 29. Acceleration trace obtained during an accelerometer calibration run

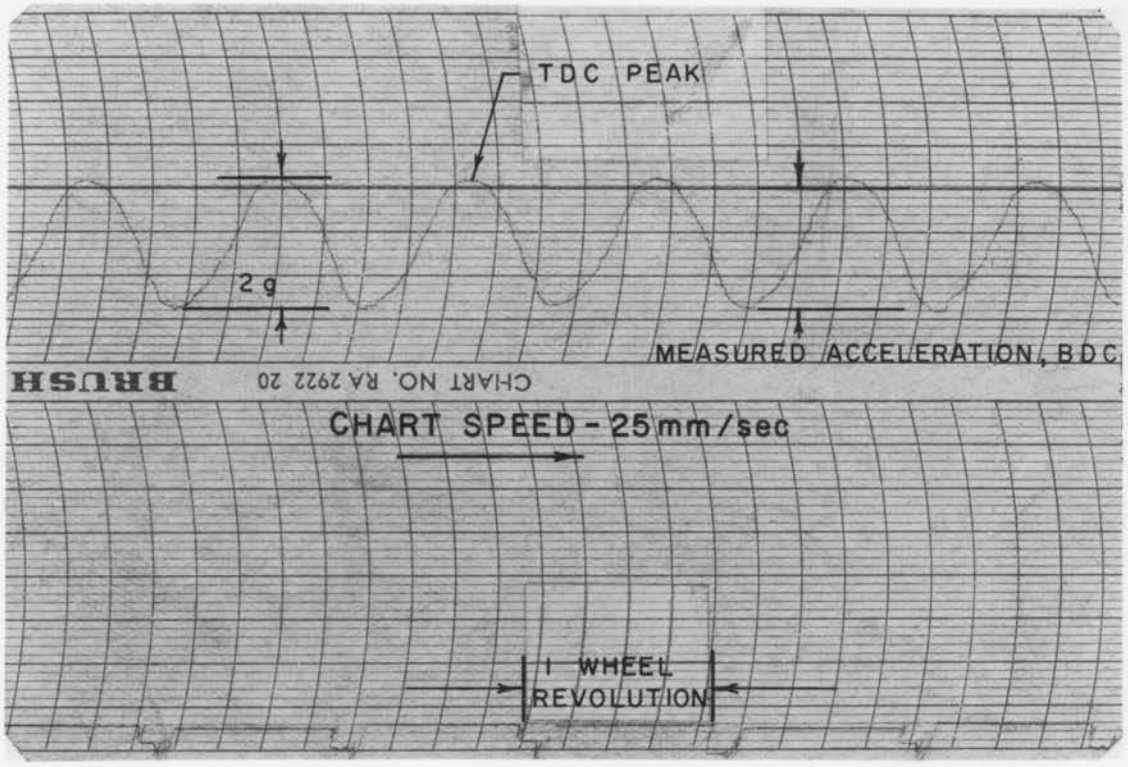
TDC PEAK
2 g
MEASURED ACCELERATION, BDC
BRUSH
CHART NO. RA 2922 20
CHART SPEED - 25 mm/sec
1 WHEEL REVOLUTION

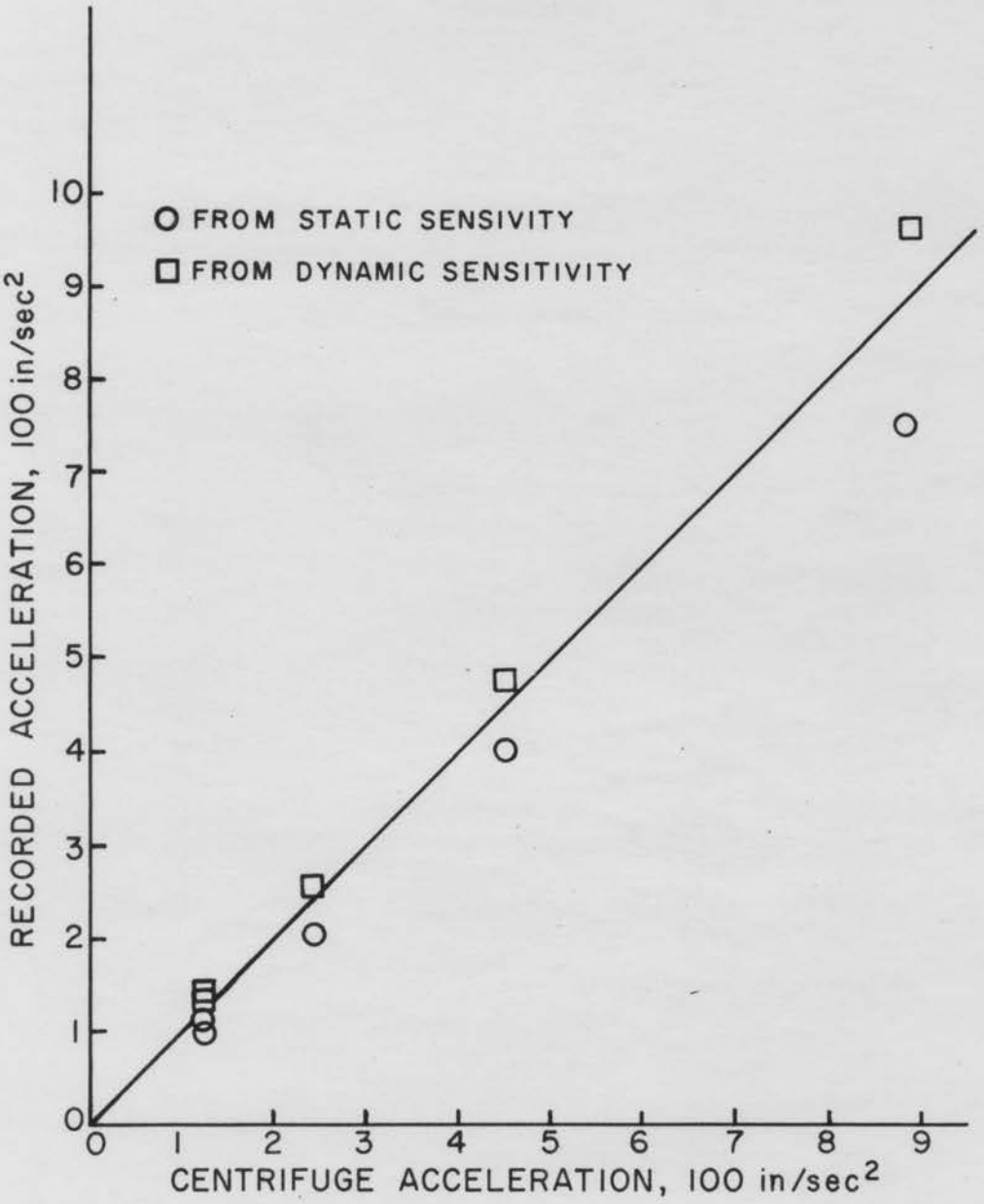

Figure 30. Results of semi-dynamic accelerometer calibration

Table 2. Results of semi-dynamic accelerometer calibration

run no.	attenuator set.	static sensitivity in/sec^2 per line	centrifuge BDC acceleration in/sec^2	recorded[a] BDC acceleration in/sec^2	recorded[b] BDC acceleration in/sec^2
1	10	50	124	100	129
2	10	50	244	205	257
3	10	50	123	113	142
4	10	50	450	400	475
5	20	100	1470	1180	1900
6	10	50	875	750	965
7	10	50	1050	880	1190
8	20	100	1340	1130	1950
9	20	100	1320	1080	1740
10	20	100	1440	1240	2180
11	50	250	3940	3470	8940
12	50	250	2200	1950	4240
13	50	250	2710	2430	4980
14	20	100	2200	1850	3180
15	50	250	3200	2750	8500
16	50	250	4110	3650	11300

[a]Based on static sensitivity.

[b]Based on dynamic sensitivity.

acceleration is indicated by the 45° line. The points based on dynamic sensitivity seem to fit the 45° line better than the points based on static sensitivity. Because of the poor results using static calibration, a final set of runs was planned in which only dynamic calibration was to be used.

Dynamic Method

For the fully dynamic calibration, the accelerometer was again initially balanced at BDC on the wheel. Then the trac-

tor was started and the wheel was allowed to achieve a uniform speed. While the wheel was rotating, the amplifier again was adjusted to give a convenient number of chart lines between the BDC and the TDC peaks. At full gain, it was not possible to attain a sensitivity of 50 in/sec^2 per line at attenuator 10. Therefore, the gain was adjusted to give a sensitivity of 100 in/sec^2 per line at attenuator 10. Leaving the gain at this setting, a full set of calibration runs were made. The results are indicated in Table 3 and in Figure 3.

The calibrate circuit in the Brush BL-320 amplifier was used to mark the final amplifier gain setting. With a 940 K resistor in the calibrate circuit and an attenuator setting of 2, a 12½ line pen deflection resulted when the calibrate switch was closed.

Table 3. Results of accelerometer final dynamic calibration

run no.	attenuator set.	static sensitivity in/sec^2 per line	centrifuge BDC acceleration in/sec^2	recorded BDC acceleration in/sec^2	error %
1	5	50	98	100	+ 2.0
2	5	50	165	165	0.0
3	5	50	310	305	- 1.6
4	5	50	393	395	+ 0.5
5	5	50	500	505	+ 1.0
6	5	50	688	685	- 0.4
7	5	50	388	400	+ 3.1
8	5	50	610	610	0.0
9	5	50	797	810	+ 1.6
10	10	100	1050	1050	0.0
11	10	100	1370	1370	0.0
12	10	100	1650	1640	- 0.6
13	20	200	1950	1980	+ 1.5

APPENDIX B: INTEGRATORS

Construction

Two identical R-C integrators of the form shown in Figure 5 were built for this study. In building the R-C circuit integrators, suitable values had to be selected for R and C.

The total impedance of each integrating circuit had to be compatible with the requirements of the preceding amplifier. The capacitor impedance in an accurate R-C integrator is negligible compared to the resistor impedance. Thus, the requirements of the preceding amplifier determine the approximate resistance value which must be used in an integrator. Resistance values of 22 Kilohms were found to be suitable.

The time constant of an R-C circuit is $t = RC$. An R-C circuit will be an accurate integrator only if the time constant is sufficiently large. On the other hand, the larger the time constant, the more the integrator attenuates the signal. A compensating amplifier is required behind each integrator to compensate for this signal attenuation.

In this study, only low gain DC amplifiers were available for compensating amplifiers. This meant the size of the integrator time constants had to be limited. The time constants, and consequently, the capacitance values had to be selected to give a suitable compromise between signal attenuation and integrator accuracy.

The circuit shown in Figure 31 was used for selecting a suitable time constant for each integrator. A 22 Kilohm resistor was used for R, and various sized capacitors were tried for C. The generator delivered a sine wave, of which the frequency could be readily changed. Thus, the attenuation factor and accuracy over any frequency range could be determined quickly for an R-C circuit with a given time constant. A 28 microfarad capacitor was selected for use with the 22 Kilohm resistor. The signal attenuation in this circuit could be adequately compensated for by the available DC amplifiers. Also, the integrator accuracy was acceptable for signal frequencies down to 1.0 cps.

A 0.33 microfarad blocking capacitor was also included in each integrator. The purpose of the blocking capacitors was to remove DC voltage components from signal. DC voltage was expected to be present due to amplifier drift and to persistent, slight misalignment of the accelerometer in the gravity field. An experiment was conducted to test the effectiveness of the blocking capacitors. The procedure and results are given in the last section of this appendix.

Calibration

After the integrators were constructed, the circuit shown in Figure 6 was used for final calibration. For explanation purposes, assume that the sine wave delivered by the generator

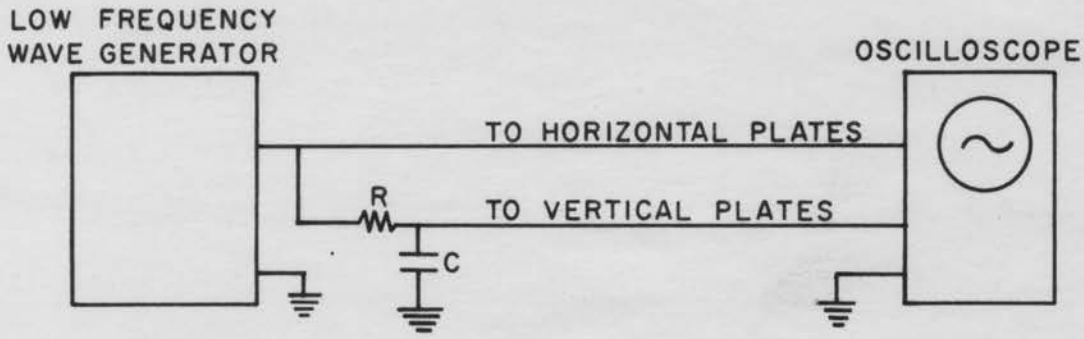

Figure 31. Circuit used for selecting a suitable integrator time constant

was an acceleration signal. The final integrator then delivered a displacement signal. These signals were recorded side by side on the oscillograph chart. The equation of the recorded acceleration wave was:

$$A = L_a \sin \omega t$$

where A was the acceleration at any time t, L_a was the acceleration amplitude in chart lines, and ω was the frequency in Radians per second. Correspondingly, the equation of the displacement trace was:

$$R = L_d \sin \omega t$$

where R was the displacement at any time t, and L_d was the displacement amplitude in lines. Since acceleration is the second derivative of displacement, the acceleration trace should also have been given by:

$$A = R\omega^2$$

or

$$A = L_d \omega^2 \sin \omega t = L_a \sin \omega t.$$

From this it follows that, at any time t:

$$L_d = \frac{L_a}{\omega^2}$$

or

$$\frac{\text{(generator output)}}{\text{(frequency)}^2\text{(integrator output)}} = \text{A constant.}$$

Thus, the purpose of the calibration was to determine this integrator constant at various frequencies.

The final compensation amplifier was equipped with a calibrated attenuator. The attenuator readings were multiples of 0.05. The above-mentioned constant ratio could be obtained with the attenuator at the first setting. For an arbitrary attenuator setting K_d, the ratio had to be

$$\left(\frac{L_a}{\omega^2 L_d}\right)\left(\frac{0.05}{K_d}\right)$$

in order to remain constant at a given frequency. Hence, the procedure for integrator calibration was to determine this ratio over the desired frequency range. The calibration results are tabulated in Table 4, and are plotted in Figure 7. The average integrator constant over this frequency range was 0.00453.

Derivation of Sensitivity

Given that:

$$\frac{0.05\ L_a}{K_d\ L_d\ \omega^2} = 0.00453$$

the next step was to derive the displacement sensitivity. If an acceleration A in/sec^2 is recorded with acceleration sensitivity S_a in/sec^2/line, then L_a will be given by:

$$L_a = \frac{A}{S_a}\ .$$

Similarly, for a displacement R inches and displacement sensitivity S_d in/line, it follows that:

Table 4. Results of the final double-integrator calibration

run no.	K_d	L_a lines	L_d lines	ω rad/sec	$\frac{0.05\ L_a}{K_d\ L_d\ \omega^2}$	frequency cps
1	0.5	37.0	14.5	7.24	0.00487	1.15
2	0.2	37.0	36.0	7.24	0.00489	1.15
3	0.2	36.5	19.0	10.28	0.00455	1.64
4	0.1	36.5	38.5	10.28	0.00448	1.64
5	0.1	36.5	23.0	13.50	0.00435	2.15
6	0.1	36.5	15.5	16.57	0.00428	2.63
7	0.05	36.5	32.0	16.57	0.00416	2.63
8	0.05	36.5	22.5	19.68	0.00418	3.13
9	0.05	36.5	16.5	23.00	0.00418	3.66
10	0.05	36.5	12.5	26.00	0.00432	4.14
11	0.05	36.5	10.0	29.25	0.00425	4.66
12	0.05	36.5	8.0	32.40	0.00434	5.16
average					0.00453	

$$L_d = \frac{R}{S_d} .$$

Putting these values into the given ratio:

$$\frac{0.05\ A/S_a}{K_d\ \omega^2\ R/S_d} = 0.00453$$

or

$$S_a = (0.00453)\left(\frac{K_d}{0.05}\right)\ S_a\left(\frac{R\omega^2}{A}\right).$$

But for the sine wave generated by the wave generator:

$$A = R\omega^2$$

therefore:

$$S_d = (0.00453)\left(\frac{K_d}{0.05}\right)S_a.$$

The acceleration sensitivity was known to be ten times the attenuator setting on the acceleration amplifier. Thus:

$$S_d = (0.0453)\left(\frac{K_d}{0.05}\right)K_a$$

where:

S_d = displacement sensitivity, inches/line

K_d = attenuator setting on final compensating amplifier

K_a = attenuator setting on acceleration amplifier.

Test of Blocking Capacitor Effectiveness

An experiment was conducted to test the effectiveness of the 0.33 μf integrator blocking capacitor in eliminating DC components from the signal. The circuitry used in the test

is shown in Figure 32. First a signal without a DC component was supplied to the integrator. A portion of the integrator input and output traces for this run are shown in Figure 33 on the chart labeled Run 1. Run 2 was a repetition of Run 1, except that a DC component was added to the integrator input. In Figure 33, the only difference between the integrator input traces is that the one for Run 2 has been shifted downward. However, the integration output traces are identical. That is, the DC component introduced in Run 2 has been completely blocked off by the blocking capacitor.

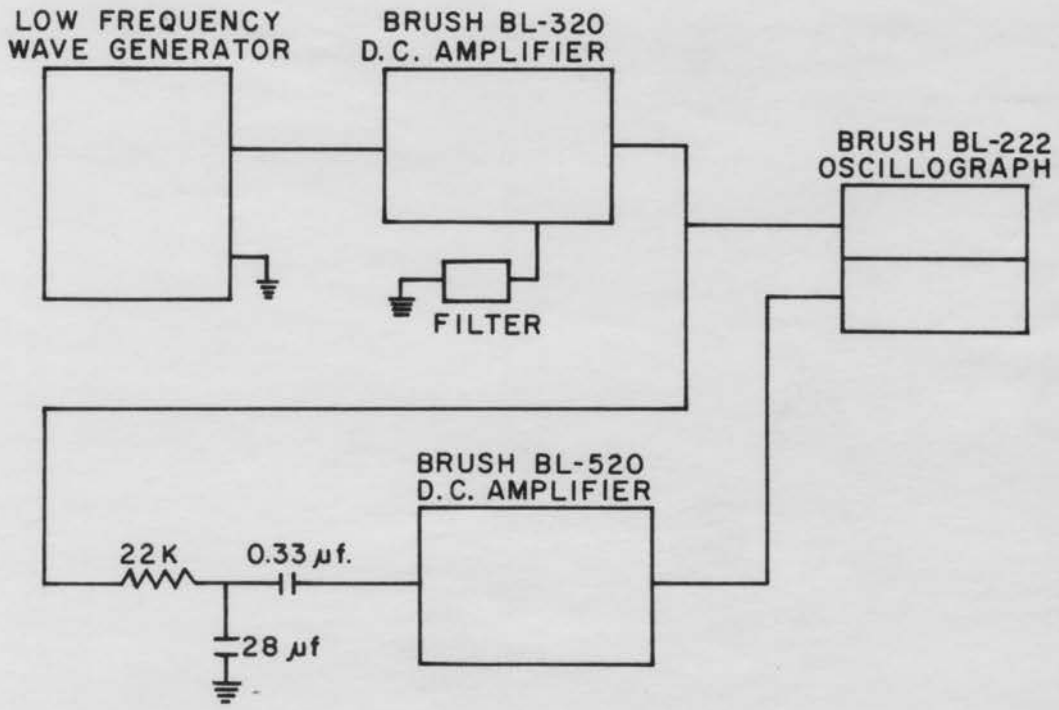

Figure 32. Circuit used for testing effectiveness of a 0.33 µf. blocking capacitor

Figure 33. An illustration of the blocking capacitor effectiveness

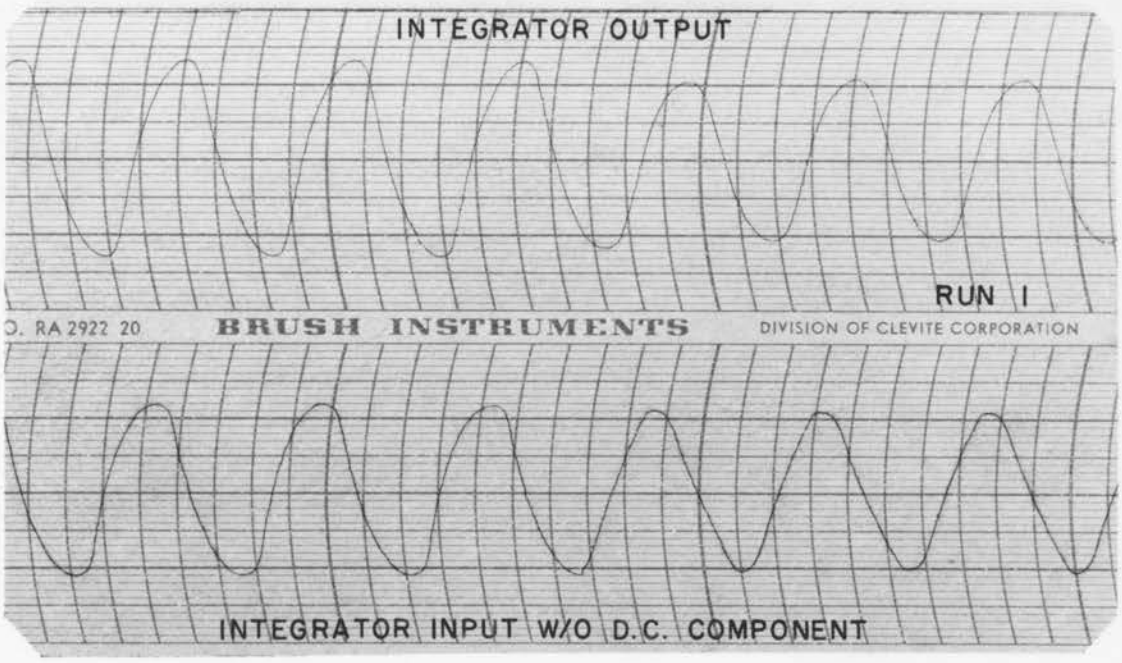
INTEGRATOR OUTPUT
RUN 1
O. RA 2922 20
BRUSH INSTRUMENTS
DIVISION OF CLEVITE CORPORATION
INTEGRATOR INPUT W/O D.C. COMPONENT

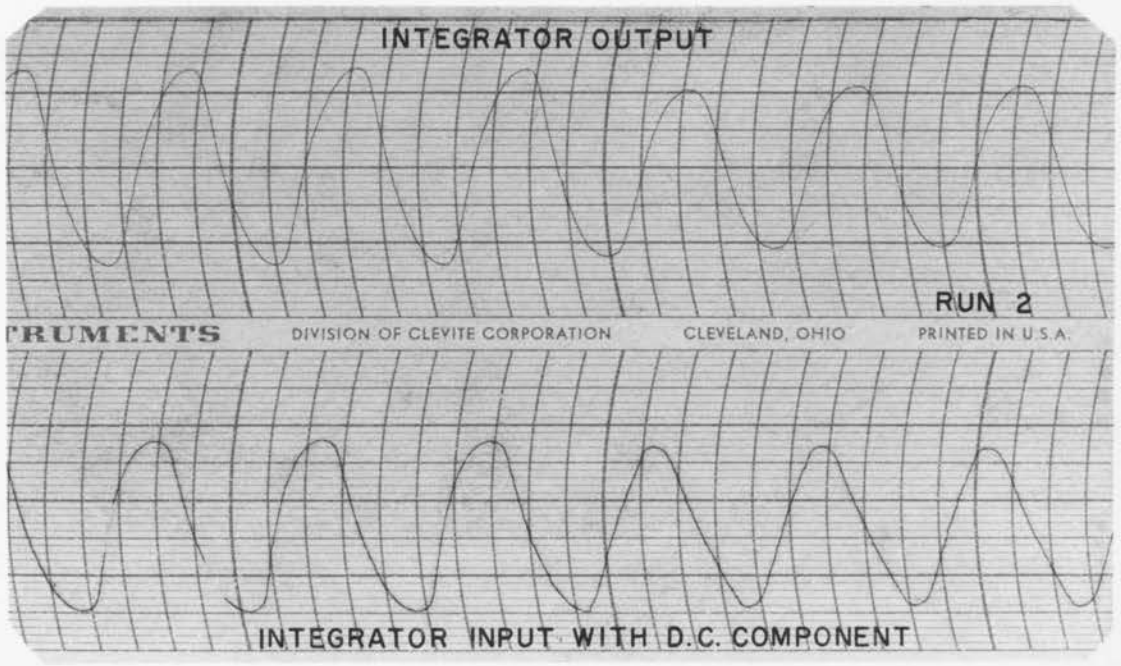
INTEGRATOR OUTPUT
RUN 2
TRUMENTS
DIVISION OF CLEVITE CORPORATION
CLEVELAND, OHIO
PRINTED IN U.S.A.
INTEGRATOR INPUT WITH D.C. COMPONENT

APPENDIX C: DESCRIPTION OF FIELDS

The fields selected for roughness measurements were as follows:

Field 1 - This field was located on the Curtiss farm north of the farmstead. On the University farms map, it is identified as field M-1. The field had been in corn continuously for at least four years previously. The normal tillage procedure for corn was fall plowing, single disking in spring, harrowing, planting and three cultivations. When roughness measurements were taken, the corn had just been picked, and the stalks shredded.

Field 2 - This field was located on the Agricultural Engineering farm, northwest of the farmstead. On the University farms map, it is identified as field D-5. As with Field 1, this field had been continuously in corn at least four years and had received the usual tillage operations. At the time roughness measurements were made, the corn had been picked, but the stalks had not been shredded. Moisture samples were taken on the ridges and between the ridges. The average moisture content of the soil on the ridges was 32% (W.B.) and between the ridges it was 31%.

Field 3 - This field was located on the Agricultural

Engineering farm, west of the farmstead. On the University farms map, it is identified as field B-5. In this field, ridges had been formed with an experimental, single-row tillage implement. The field had then been planted to red clover. When the roughness measurements were taken, the field had a heavy vegetative cover on it. The soil moisture content on the ridges was 26%, between the ridges, 29%.

Field 4 - This was the same as field 1, after fall plowing had occurred. The fall plowing had been done while the field was wet, and consequently, the plowed surface was quite rough. One rain had fallen since plowing which had only slightly softened the clods. The soil below the clod level was at 29% moisture, but the surface clods contained only 19% moisture. Thus, at the time roughness measurements were taken, this field was considered to represent a condition of severe roughness.

Field 5 - This field was located on the Swine Nutrition farm, north of the farmstead. On the University farms map, it is identified as field H-11. This field had been in alfalfa pasture for several years previously. It had been plowed during the summer, and numerous rains had fallen on it since plowing.

At the time roughness measurements were taken, this field was considered only mildly rough.

Field 6 - This field was located on the Agricultural Engineering farm in the area reserved for student class work. On the University farms map, it is identified as field D-4. Soybeans had been planted the previous year, and the current soybean crop had just been combined. The tillage sequence for the soybeans was fall plowing, spring single disking, planting, and two cultivations. The moisture content of the ridges was 31%, and the moisture content between the ridges was 25%.

Field 7 - This field was north of and adjacent to Field 6. On the University farms map, it is identified as field D-2. The previous fall, the field had been fall plowed. This was followed by single disking in the spring, after which oats crop had been removed. The average soil moisture content was 29%. This meadow was considered to represent a fairly smooth field surface.

APPENDIX D: FIELD DATA SHEET

FIELD ROUGHNESS DATA

Name of Recorder _____

Date _____

Name of Driver _____

Field Location _____

Field Number _____ Soil Moisture _____%

Tractor Front Tire Pressure _____

Bicycle Tire Pressure _____

Tractor Gear _____ Overdrive set. _____

Speed _____mph.

Direction of travel with respect to rows, plowing direction, furrows, etc. _____

_____

Run No. on data chart _____

Acceleration Amplifier:

Attenuator Setting _____

Sensitivity at this setting _____ $in/sec^2/line$

Displacement Amplifier:

Attenuator setting _____

Sensitivity at this setting _____ in/line

Chart Speed _____mm/sec

Accelerometer mounted on _____

Filter used _____

APPENDIX E: DETERMINATION OF EFFECTIVE WHEEL CIRCUMFERENCE

The data analyses required a knowledge of the relationship between oscillograph chart distance and horizontal distance in the field. The event marker system provided a record of the number of millimeters of chart per wheel revolution. This left the problem of finding the forward inches of travel per wheel revolution, i.e., the effective wheel circumference. The effective circumference was measured by driving the tractor over a cinder track. A chain tied around the front wheel left a mark each wheel revolution. The average distance between marks was then determined with an ordinary surveying tape. Thus, the average effective circumference was found to be 87.3 inches.

The effective circumference was one of the factors used in determining wavelengths in row crop fields. The average wavelength in these fields is approximately 40 inches. However, when certain runs were analyzed, the average wavelength was found to be as much as 12% low. The cause was found to be slippage of the wheel on which the event marker switch was mounted. This was also the wheel on which the tire feeler device was sometimes mounted. The drag of the tire feeler assembly was sufficient to slow the wheel down, giving a longer effective circumference. Thus for certain runs another means had to be found for estimating the effective wheel circumfer-

ence.

In the row crop fields where the tire feeler device was used, an effective circumference was selected which would make the row spacing average out to 40 inches. A check on these estimates was available. In a given field, the tractor speeds on various runs should have been quite close, since the throttle setting was marked for maintaining constant speed. Using the estimated circumferences, the largest difference between speeds was calculated to be only 3%. Thus, the estimates of effective wheel circumference were good.

In the non-row crop fields, there were no known ground features on which to base estimates of the effective wheel circumference. The procedure followed there was to assume the tractor speed equal to the speed for a similar run in the same field without the tire feeler device. By making this assumption, it was then possible to estimate the effective wheel circumference for the run where the tire feeler device was used.

APPENDIX F: ROUGHNESS DATA FROM ROW CROP FIELDS

Table 5. Results of roughness measurements in Field 1

wave[a] no.	wavelengths L, inches	wavelengths group statistics	average tractor speeds, mph	harmonic analyses constant terms b_o inches	harmonic analyses constant terms b_o-b_o(min) inches	wave double amplitudes amplitudes, inches	wave double amplitudes group statistics
1F1-1	46.2			3.39	0.55	2.26	
1F1-2	36.6	m=40.0"		2.84	0.00	2.85	m=2.68"
1F1-3	40.9	s=9.1"	3.1	2.96	0.12	3.44	s=1.10"
1F1-4	35.5	C=23%		3.37	0.53	2.06	C=41%
1F1-5	41.9			3.92	1.08	2.88	
1F1-6	38.7			3.78	0.94	2.61	
1B1-1	37.4			3.55	1.11	2.05	
1B1-2	40.8	m=40.5"		3.39	0.95	2.20	m=2.33"
1B1-3	43.1	s=4.7"	3.2	3.18	0.74	3.34	s=1.42"
1B1-4	42.0	C=12%		3.32	0.88	2.92	C=61%
1B1-5	38.6			3.17	0.73	1.68	
1B1-6	40.8			2.44	0.00	1.77	
1A1-1	40.9			3.67	0.52	2.55	
1A1-2	37.6	m=39.4"		4.21	1.06	2.16	m=2.56"
1A1-3	40.9	s=8.5"	3.1	3.72	0.57	3.06	s=1.32"
1A1-4	34.3	C=22%		3.63	0.48	2.46	C=52%
1A1-5	45.3			3.15	0.00	3.48	
1A1-6	37.6			3.27	0.12	1.75	

[a]The number-letter-number combination before the dash is the run number. The first number is the field number. The letter denotes the accelerometer location during the run. F indicates tire feeler device, B indicates bicycle wheel and A indicates tractor axle. The next number distinguishes between repeated runs. The number after the dash identifies a wave within a run.

Table 6. Cosine coefficients from harmonic analyses of waves in Field 1

wave[a] number	cosine harmonic amplitudes as % of total wave amplitudes							
	b_1	b_2	b_3	b_4	b_5	b_6	b_7	b_8
1F1-1	93	33	5	4	3	2	2	1
1F1-2	96	4	-2	-2	-1	0	1	-1
1F1-3	75	14	-9	5	-1	-2	-1	0
1F1-4	97	28	-4	-1	1	1	0	-2
1F1-5	77	10	1	-1	-1	-2	-3	0
1F1-6	82	11	2	6	1	2	4	3
1B1-1	109	12	-4	2	-2	2	3	1
1B1-2	54	20	-6	2	3	2	1	0
1B1-3	84	-15	-5	-2	0	-4	0	-2
1B1-4	80	7	4	5	1	-1	-2	1
1B1-5	88	10	12	7	7	1	4	1
1B1-6	85	18	3	2	1	-2	0	0
1A1-1	102	22	-2	-5	-1	-1	0	0
1A1-2	97	-18	6	1	-2	2	0	0
1A1-3	99	3	-5	-3	0	-1	1	0
1A1-4	102	20	-4	-4	0	1	2	2
1A1-5	85	-14	14	-2	3	0	0	1
1A1-6	104	- 8	1	6	-2	0	0	0

[a]For explanation of wave number, see Table 5.

Table 7. Sine coefficients from harmonic analyses of waves in Field 1

wave[a] number	sine harmonic amplitudes as % of total wave amplitudes							
	a_1	a_2	a_3	a_4	a_5	a_6	a_7	a_8
1F1-1	27	19	17	9	6	6	4	5
1F1-2	-29	12	- 1	-2	-1	1	1	0
1F1-3	-28	25	- 9	-5	2	-3	0	-1
1F1-4	-5	-7	- 9	-5	-1	-1	-1	-2
1F1-5	-59	12	- 3	-5	-4	-3	-1	-2
1F1-6	-6	48	6	13	8	5	5	3
1B1-1	26	17	1	5	9	0	2	3
1B1-2	-78	29	14	5	4	3	5	0
1B1-3	-57	22	-11	-1	-6	0	-4	-1
1B1-4	-35	33	5	0	-1	-1	-2	0
1B1-5	54	11	22	12	13	7	9	4
1B1-6	-40	1	-5	1	3	0	0	0
1A1-1	-12	2	3	3	1	0	0	-1
1A1-2	0	-3	5	1	1	1	-1	0
1A1-3	-17	13	-4	3	0	-1	0	0
1A1-4	34	1	-3	5	5	2	0	0
1A1-5	-31	32	-1	1	7	0	4	0
1A1-6	-10	-3	10	4	0	2	2	1

[a]For explanation of wave numbers, see Table 5.

Table 8. Results of roughness measurements in Field 2

wave[a] no.	wavelengths: L, inches	wavelengths: group statistics	average tractor speeds, mph	harmonic analyses constant terms: b_o inches	harmonic analyses constant terms: $b_o - b_o(\min)$ inches	wave double amplitudes: amplitudes, inches	wave double amplitudes: group statistics
2B1-1	37.2			1.76	0.00	1.70	
2B1-2	40.3	m=39.6"		2.11	0.35	2.92	m=2.58"
2B1-3	39.3	s=4.0"	2.9	2.04	0.28	2.42	s=1.49"
2B1-4	38.3	C=10%		2.10	0.34	3.36	C=58%
2B1-5	40.3			2.14	0.38	3.15	
2B1-6	42.4			1.80	0.04	1.96	
2B2-1	38.9			2.94	0.00	3.67	
2B2-2	45.2	m=39.9"		3.11	0.17	2.40	m=2.31"
2B2-3	37.8	s=8.5"	3.0	3.20	0.26	2.21	s=1.70"
2B2-4	35.7	C=21%		3.96	1.02	1.52	C=74%
2B2-5	37.8			3.90	0.96	2.29	
2B2-6	44.1			3.92	0.98	1.75	
2B3-1	41.4			3.02	1.86	1.86	
2B3-2	44.6	m=41.8"		3.67	2.31	2.31	m=2.14"
2B3-3	35.0	s=9.0"	3.0	4.11	2.29	2.29	s=0.40"
2B3-4	45.7	C=22%		3.95	2.22	2.22	C=19%
2B3-5	39.3			3.68	2.18	2.18	
2B3-6	44.6			3.50	1.99	1.99	

[a]For explanation of wave numbers, see Table 5.

Table 9. Cosine coefficients from harmonic analyses of waves in Field 2

wave[a] number	cosine harmonic amplitudes as % of total wave amplitudes							
	b_1	b_2	b_3	b_4	b_5	b_6	b_7	b_8
2B1-1	94	10	6	-2	0	1	0	-1
2B1-2	71	-2	2	-3	-1	-2	1	-2
2B1-3	101	5	-5	2	-1	0	1	2
2B1-4	76	6	-12	1	-1	-1	-1	-2
2B1-5	90	-7	8	-5	1	1	2	3
2B1-6	86	26	-5	0	-3	1	0	2
2B2-1	97	-21	2	0	-1	0	1	0
2B2-2	88	0	13	-6	2	-1	3	-1
2B2-3	98	10	-10	-5	-2	-3	-4	-1
2B2-4	101	9	-1	-2	1	1	1	0
2B2-5	93	-15	7	-7	1	1	-2	-1
2B2-6	83	19	2	-1	1	1	0	1
2B3-1	88	-1	6	-9	1	-4	1	-3
2B3-2	53	26	-8	-5	-2	-1	-4	-1
2B3-3	98	-1	-2	-4	-2	0	-3	-1
2B3-4	97	25	-10	1	3	-1	0	2
2B3-5	98	-12	6	0	0	4	1	0
2B3-6	93	-16	1	0	3	0	0	1

[a]For explanation of wave numbers, see Table 5.

Table 10. Sine coefficients from harmonic analyses of waves in Field 2

wave[a] number	sine harmonic amplitudes as % of total wave amplitudes							
	a_1	a_2	a_3	a_4	a_5	a_6	a_7	a_8
2B1-1	-51	-7	12	-1	2	0	2	-1
2B1-2	-63	29	-10	-1	-4	-3	-2	0
2B1-3	-5	24	2	-4	6	3	0	2
2B1-4	-54	11	-9	-7	0	-3	-2	-3
2B1-5	29	4	17	-2	4	4	2	3
2B1-6	-3	29	-6	0	2	2	2	1
2B2-1	-11	1	1	0	-2	0	-1	0
2B2-2	16	25	-2	3	0	4	3	3
2B2-3	-40	-34	6	-3	-6	-7	-2	-2
2B2-4	-8	2	7	2	-1	0	1	1
2B2-5	6	-7	-2	2	-3	-1	1	-1
2B2-6	-29	37	18	1	0	4	2	3
2B3-1	-27	13	-10	-8	-5	-3	-1	-1
2B3-2	-70	19	-16	-8	-5	0	-3	-3
2B3-3	-49	5	5	-6	-3	-2	-2	0
2B3-4	10	30	3	5	2	1	3	2
2B3-5	35	1	0	10	1	3	2	-1
2B3-6	-4	30	-3	0	2	5	1	0

[a]For explanation of wave numbers, see Table 5.

Table 11. Results of roughness measurements in Field 3

wave[a] no.	wavelengths L, inches	wavelengths group statistics	average tractor speeds, mph	harmonic analysis constant terms b_o inches	harmonic analysis constant terms b_o-b_o(min) inches	wave double amplitudes amplitudes, inches	wave double amplitudes group statistics
3B1-1	56.1			2.20	0.39	2.98	
3B1-2	38.5	m=41.6"		1.95	0.14	3.38	m=2.80"
3B1-3	36.3	s=17.1"	3.1	2.14	0.33	3.04	s=0.98"
3B1-4	37.4	C=41%		2.39	0.58	2.45	C=35%
3B1-5	37.4			1.86	0.05	2.82	
3B1-6	44.0			1.81	0.00	2.15	

[a]For explanation of wave numbers, see Table 5.

Table 12. Cosine coefficients from harmonic analyses of waves in Field 3

wave[a] number	cosine harmonic amplitudes as % of total wave amplitudes							
	b_1	b_2	b_3	b_4	b_5	b_6	b_7	b_8
3B1-1	79	12	-14	4	1	-3	-2	1
3B1-2	97	-12	3	-3	2	-1	0	1
3B1-3	98	-8	-1	-2	-3	1	-1	-1
3B1-4	100	2	-6	3	0	0	0	1
3B1-5	91	-12	1	3	1	2	4	1
3B1-6	95	-36	8	5	-7	2	-3	-2

[a]For explanation of wave numbers, see Table 5.

Table 13. Sine coefficients from harmonic analyses of waves in Field 3

wave[a] number	sine harmonic amplitudes as % of total wave amplitudes							
	a_1	a_2	a_3	a_4	a_5	a_6	a_7	a_8
3B1-1	-43	18	-4	1	0	1	1	-1
3B1-2	-17	7	6	-1	1	-1	1	0
3B1-3	-15	-14	6	-4	0	-1	-2	-1
3B1-4	20	-8	7	6	-1	0	0	1
3B1-5	46	0	20	0	5	4	2	3
3B1-6	-2	-27	-5	1	-10	1	-4	-1

[a]For explanation of wave numbers, see Table 5.

Table 14. Results of roughness measurements in Field 6

wave[a] no.	wavelengths L, inches	wavelengths group statistics	average tractor speeds,	harmonic analyses constant terms b_o inches	harmonic analyses constant terms $b_o-b_o(min)$ inches	wave double amplitudes amplitudes, inches	wave double amplitudes group statistics
6F1-1	39.0			1.72	0.23	1.89	
6F1-2	41.0	m=40.0"		2.00	0.51	1.91	m=2.44"
6F1-3	37.9	s=4.3"	3.1	1.83	0.34	2.67	s=1.00"
6F1-4	40.0	C=11%		1.49	0.00	3.01	C=41%
6F1-5	39.0			1.75	0.26	2.62	
6F1-6	43.3			1.87	0.38	2.52	
6A1-1	40.2			1.57	0.00	1.77	
6A1-2	37.0	m=40.0"		1.66	0.09	1.77	m=2.29"
6A1-3	39.1	s=5.7"	3.1	1.62	0.05	2.41	s=1.09"
6A1-4	40.2	C=14%		1.63	0.06	3.01	C=47%
6A1-5	39.1			1.67	0.10	2.59	
6A1-6	44.6			1.76	0.19	2.20	
6B1-1	39.1			1.95	0.42	1.58	
6B1-2	40.2	m=40.0"		1.96	0.43	1.29	m=2.03"
6B1-3	38.0	s=3.7"	3.2	1.67	0.14	2.13	s=1.65"
6B1-4	41.4	C=9%		1.68	0.15	1.37	C=81%
6B1-5	39.1			2.21	0.68	2.86	
6B1-6	42.5			1.53	0.00	2.96	

[a]For explanation of wave numbers, see Table 5.

Table 15. Cosine coefficients from harmonic analyses of waves in Field 6

wave[a] number	cosine harmonic amplitudes as % of total wave amplitudes							
	b_1	b_2	b_3	b_4	b_5	b_6	b_7	b_8
6F1-1	106	28	-4	-3	0	3	1	1
6F1-2	91	7	-6	-5	-3	-5	0	0
6F1-3	96	5	2	-2	3	-4	0	1
6F1-4	77	26	4	2	-3	0	0	-1
6F1-5	98	-13	5	0	-3	1	0	0
6F1-6	52	52	-10	-8	-2	0	0	-2
6A1-1	70	15	-1	-4	-1	-3	0	1
6A1-2	105	5	-5	-3	-2	-1	-1	-1
6A1-3	88	38	-7	-10	-1	0	-2	-2
6A1-4	99	-2	3	-1	0	0	0	1
6A1-5	100	2	-6	-1	1	1	-1	0
6A1-6	91	-17	12	0	-2	3	0	0
6B1-1	85	17	0	2	8	-1	-4	3
6B1-2	83	3	10	-13	4	0	1	-2
6B1-3	91	-5	7	-1	1	-1	1	0
6B1-4	102	12	-15	-17	-3	-6	-1	-2
6B1-5	90	-7	-3	-4	1	0	1	0
6B1-6	89	18	1	-5	-2	1	4	-1

[a]For explanation of wave numbers, see Table 5.

Table 16. Sine coefficients from harmonic analyses of waves in Field 6

wave[a] number	sine harmonic amplitudes as % of total wave amplitudes							
	a_1	a_2	a_3	a_4	a_5	a_6	a_7	a_8
6F1-1	11	10	10	7	4	3	3	1
6F1-2	-26	3	-22	-3	-4	-1	-3	-1
6F1-3	-37	9	4	-1	1	1	2	-1
6F1-4	-13	31	-9	-1	0	1	1	1
6F1-5	-22	1	9	-1	1	1	-1	1
6F1-6	-51	25	-17	10	-1	2	-2	-2
6A1-1	-64	24	-6	1	-4	-2	-3	-1
6A1-2	-23	-9	4	-1	-2	-3	-3	-1
6A1-3	5	-13	-10	1	0	-4	-2	-1
6A1-4	-11	7	2	5	0	0	2	1
6A1-5	-21	11	2	3	2	0	0	2
6A1-6	10	6	7	-2	4	2	1	2
6B1-1	56	19	2	8	-4	0	5	1
6B1-2	-6	12	-26	-12	8	3	-3	-6
6B1-3	-20	13	-1	3	2	0	0	-1
6B1-4	2	-40	-38	-19	4	-4	-8	-5
6B1-5	14	15	-11	7	-1	3	-2	2
6B1-6	16	33	-21	4	5	4	-1	2

[a]For explanation of wave numbers, see Table 5.

APPENDIX G: ROUGHNESS DATA FROM NON-ROW CROP FIELDS

Table 17. Distribution of obstructions encountered in Run 4F1 with tractor speed of 2.8 mph

obstruction spacing, inches	% of spacings > indicated spacing if minimum obstruction height is:				
	0.18"	0.36"	0.72"	1.09"	1.81"
2.0					
4.0					
6.0					
8.0					
10.0	100				
12.0	99				
14.0					
16.0					
18.0	97				
20.0	93	100			
22.0	90	98	100	100	
24.0	85	94	95	94	
26.0	80	90	93	92	
28.0	70	83	89	89	
30.0	62	81	87		
32.0	56	75	84		100
34.0	49	69	80	83	96
36.0	44	65	78	80	92
38.0	36	60	76	77	
40.0	29	50	71	72	88
42.0	24	44	64	66	83
44.0	21	42	62	63	
46.0	20				
48.0	18	40	60	60	
50.0	17	36	56	57	79
52.0	15	35	53	54	
54.0	14	33	51	51	75
56.0		31			
58.0	12	27	49		
60.0	11	21	40	46	
62.0	9	19	38	43	
64.0	8	17	36		
66.0		15	24	37	
68.0					
70.0	6	13	22	34	71
72.0	5	10	20	29	67
74.0	3				
76.0	2	8			63
78.0		6	18	26	58
80.0					

Table 17. (Continued)

obstruction spacing, inches	% of spacings > indicated spacings if minimum obstruction height is:				
	0.18"	0.36"	0.72"	1.09"	1.81"
82.0					54
84.0					
86.0					50
88.0		4	16	23	42
90.0	0	2	13	20	
92.0					
94.0					38
96.0			11	17	33
98.0			7	14	
100					
102					
104					
106					
108					
110					
112			4	11	
114			2	9	29
116					25
118					
120					
122					
124					
126					21
128					17
130					
132					13
134		0	0	6	
136					
138					
> 138				3	8

Table 18. Distribution of obstructions encountered in Run 5F1 with tractor speed of 3.0 mph

obstruction spacing, inches	% of spacings > indicated spacing if minimum obstruction height is:					
	0.09"	0.18"	0.36"	0.54"	0.91"	1.27"
2.1						
4.2						
6.3						
8.4	100					
10.5	98					
12.6	97					
14.7	95	100				
16.8	94	98				
18.9	86	96				
21.0	83	94				
23.1	75	92	100	100		
25.2	73	86	96	97		
27.3	66	84	93	94	100	
29.4	55	76	87	89	96	100
31.5	48	65	76	80	92	95
33.6	38	63				
35.7	33	55	67	69	85	90
37.8	31	47	61			
39.9	28	43	57			
42.0	27	39	48	63	81	85
44.1	22	37	46			
46.2	19	33	41	54	77	80
48.3	16	29	37			
50.4	14	27	35			
52.5	11	24	33	51		
54.6	6	20	26	46		
56.7	3	18	24			
58.8	2		22			
60.9	0	16	17	43	69	75
63.0		12		40		
65.1				37	65	
67.2					58	
69.3		10	13	34	54	70
71.4		6	9	29	46	65
73.5		4	7	26	42	60
75.6						
77.7		2	4	23	38	50
79.8						
81.9		0	0			
84.0						
86.1				20	35	45
88.2				17		

Table 18. (Continued)

obstruction spacing, inches	% of spacings > indicated spacing if minimum obstruction height is:					
	0.09"	0.18"	0.36"	0.54"	0.91"	1.27"
90.3						
92.4				14	27	35
94.5						
96.6						
98.7						
101						30
103				11	19	
105						
107						
109						
111						
113						
116				9	15	25
118						20
120						
122				6		
124						
126				3	12	15
128						
130						
132						
134						
137						
139				0		
141						
143						
145						
> 145					8	10

Table 19. Distribution of obstructions encountered in Run 7F1 with tractor speed of 3.3 mph

obstruction spacing, inches	% of spacings > indicated spacing if minimum obstruction height is: 0.09"	0.18"	0.36"	0.54"	0.91"
2.3	100	100			
4.6	99	98			
7.0					
9.3	96				
11.6	95				
13.9	92				
16.2	89				
18.6	87				
20.9	83	93			
23.2	73	87			
25.5	68	85	100	100	
27.8	59	79	93	97	
30.2	56	75			
32.5	45	69	89	95	
34.8	40	61	85		100
37.1	36	56	83	92	96
39.4	29	49	76	87	
41.8	23	43	67	76	91
44.1	19	34	61	71	86
46.4	13	26	54	66	82
48.7					
51.0	11	23	52		
53.4	9	21	50		
55.7	8	20	48	63	
58.0	7	18	46	60	
60.3	5	15	41	58	
62.6			39	53	
65.0		10	30	45	77
67.3		8	24	39	
69.6	4	7	20	34	68
71.9					
74.2	1	3	13	29	
76.6		2	11	26	
78.9			9	21	
81.2			7	18	
83.5					
85.8					
88.2			4		

Table 19. (Continued)

obstruction spacing, inches	% of spacings > indicated spacing if minimum obstruction height is: 0.09"	0.18"	0.36"	0.54"	0.91"
90.5	0	0	2	13	59
92.8					
95.1					55
97.4					
99.8					
102					
104				11	46
107					
109					41
111					
114					
116					
118					
121					
123				8	
125					
128				5	36
130					32
132				3	27
135			0		
137					23
139				0	
142					
144					18
146					
148					
151					
153					
155					
> 155					14

Table 20. Distribution of obstructions encountered in Run 7F2 with tractor speed of 6.6 mph

obstruction spacing, inches	% of spacings > indicated spacing if minimum obstruction height is: 0.23"	0.45"	0.91"	1.36"
4.6				
9.3				
13.9				
18.5				
23.2	100			
27.8	96	100	100	
32.4	89	92	96	
37.0	74	83		100
41.7	55	64	83	88
46.3	47	58		
50.9	40	56		
55.6	36			
60.2	25	44	70	82
64.8	21	39	61	
69.5	15	36		
74.1	13			
78.7	11	31		
83.3			57	
88.0	9			
92.6	4	22	48	76
97.2				
102				71
107		19	44	
111	2	17	35	65
116		14		
120				
125	0			59
130			30	53
134				
139		11	26	
144		8	22	
148				47
153				41
157		6		
> 157		3	17	35